Hindawi
Journal of Chemistry
Volume 2024, Article ID 2013446, 25 pages
https://doi.org/10.1155/2024/2013446

Research Article

Antibacterial and Antioxidant Activities of Triterpenoids and Cyclic 1,7-Diarylheptanoids from the Stem Bark of *Myrica salicifolia*: A Combined Experimental and Computational Study

Abraham Dilnesa Gashaw,[1] **Kibrom Gebreheiwot Bedane**,[1] **Taye B. Demissie**,[2] **Japheth O. Ombito**,[2] **Estifanos Ele Yaya**,[1] **and Mekonnen Abebayehu Desta**[1]

[1]*Department of Chemistry, College of Natural and Computational Sciences, Addis Ababa University, P.O. Box 1176, Addis Ababa, Ethiopia*
[2]*Department of Chemistry, University of Botswana, P/Bag UB 0022, Gaborone, Botswana*

Correspondence should be addressed to Estifanos Ele Yaya; estifanose.ele@aau.edu.et and Mekonnen Abebayehu Desta; mekonnen.abebayehu@aau.edu.et

Received 25 July 2023; Revised 9 January 2024; Accepted 18 January 2024; Published 12 February 2024

Academic Editor: Liviu Mitu

Myricasalicifolia A Rich (Myricaceae) is a tree growing in Central and East Africa. Traditionally, the plant is used to treat malaria, respiratory disorders, inflammations, and infections. A new compound, 3β-O-trans-caffeoylisomyricadiol (7), was isolated from MeOH : $CHCl_3$ (2 : 1) extract of the stem bark of *Myrica salicifolia* along with seven known compounds, namely, myricanone (**1**), myricanol (**2**), myricanol-11-*O*-β-D-xylopyranoside (**3**), taraxerone (**4**), taraxerol (**5**), myricadiol (**6**), and methyl-β-D-glucopyranoside (**8**). This is the first report of the isolation of taraxerene-type triterpenes from this plant. The structures were determined by a comprehensive analysis of 1D/2D NMR spectroscopy, HR-MS, and by comparison with literature data. The compounds showed a wide range of DPPH scavenging activities from very weak (IC_{50} value = 282.61 μM) to very strong (IC_{50} = 13.48 μM). Antibacterial activities of the compounds were evaluated using the disk diffusion agar method, where some of the compounds showed modest antibacterial activities against *S. pyogenes* and *S. aureus* at 250 μg/mL. Compounds **2**, **3**, and **7** were assessed for their *in silico* molecular docking analysis. The lowest binding affinity for compound **7** was found to be −7.26 to −10.35 kcal/mol against PqsA protein of *P. aeruginosa*, pyruvate kinase (PK) enzyme of *S. aureus*, LuxS protein of *S. pyogenes*, and DNA gyrase B of *E.* coli, which showed better binding affinity compared to the standard drug ampicillin (−7.36 to −8.03 kcal/mol) and ciprofloxacin (−6.19 to −6.83 kcal/mol). *In silico* ADMET predictions revealed that compounds **3** and **8** met all the requirements for pharmacokinetic properties.

1. Introduction

Myrica salicifolia A Rich (Myricaceae) is a deciduous shrub with a trunk diameter of up to 1 m and typically 3–10 meters tall and can grow up to 20 meters in height. It is found in Central and East Africa, including Ethiopia, Zambia, Kenya, Burundi, Malawi, Uganda, Madagascar, Zaire, Rwanda, Tanzania, and also in Saudi Arabia [1, 2]. In Ethiopia, it is known by the local names "*Shinet*" or "*Kalava*" in Amharic, "*Abay*," "*Kataba*," "*Radji*" or "*Tona*" in Affan Oromo, and "*Nihibi*" in Tigrigna [3, 4]. The plant has a long history of use as a traditional medicine in Tanzania, where it is used to treat a variety of illnesses, including pneumonia, chronic constipation, cryptococcal meningitis, herpes zoster, stomach pain, and headaches [5, 6]. *M. salicifolia* has also been used to treat erectile dysfunction and male sexual impotence in Uganda [7]. In Ethiopia, it is used to treat lung diseases, inflammation, and skin diseases [8].

Compounds isolated from *M. salicifolia* have shown a range of biological activities. Marealle et al. reported the antimycobacterial activity of compounds isolated from *M. salicifolia* against three nonpathogenic mycobacterial species. Maslinic acid showed the highest MICs value of 17, 28, and 56 μg/mL against *Mycobacterium madagascariense*,

standard *Mycobacterium tuberculosis* strain $H_{37}RV$, and rifampicin-resistant *M. tuberculosis* clinical isolates, respectively [9]. It has been linked to antimalarial [4], antiplasmodial [10], strong analgesic effects [11], and lowering blood glucose effects [12]. Recently, Rehman and coworkers reported that the root extract of *M. salicifolia* inhibited the activation of IL-6 and TNF-α in the colonic tissues of the UC model in rats [13]. A preliminary phytochemical analysis of its stem bark [3], root [4], and leaves [14] revealed the presence of polyphenols, saponins, glycosides, unsaturated sterols, triterpenes, alkaloids, tannins, flavonoids, proteins, and carbohydrates. Several cyclic diarylheptanoids were isolated from a methanolic extract of *Morella salicifolia* bark [15].

The objectives of this study include a comprehensive phytochemical investigation of the stem bark, assessment of antibacterial and antioxidant properties of the isolated compounds, and *in silico* molecular docking study of the isolated compounds against PqsA of *P. aeruginosa*, pyruvate kinase (PK) of *S. aureus*, LuxS of *S. pyogenes*, and DNA gyrase B of *E. coli*.

2. Materials and Methods

2.1. General Experimental Procedures. NMR experiments (1D and 2D) were recorded on a 600.0 MHz Bruker Avance III spectrometer using DMSO, MeOD, $CDCl_3$ solvents, and TMS as an internal reference. Mass spectra were recorded on a high-resolution mass spectrometer (Thermo Scientific, USA) equipped with an electrospray ionization (ESI) ion source. The matrix-assisted laser desorption/ionization high resolution mass spectrometry (MALDI-HR-MS) was conducted using an Applied Biosystems 4800 Proteomics Analyzer equipped with an Nd/YAG laser ($\lambda = 335$ nm), operated at a repetition rate of 200 Hz on a Bruker New ultrafleXtremeTM instrument. FT-IR (PerkinElmer) in the range 4000–400 cm^{-1} (resolution: 4 cm^{-1}, number of scans: 4) was used using KBr discs. For column chromatography, silica gel 60 (70–230 mesh ASTM) and Sephadex LH−20 (18–111 μm, GE Healthcare Bio-Sciences AB, Sweden) were used. The isolation process was monitored by TLC (precoated sheets, ALUGRAM, Xtra SIL G/UV_{254}, 20 × 20 cm, coated with silica gel 60 fluorescent indicator, Germany), which was visualized under UV light and also sprayed with vanillin and/or cerium molybdate stain followed by heating gently for a few seconds.

2.2. Plant Material. The stem bark of *M. salicifolia* was collected from Debre Sina, Northern Shewa, Amhara region, 192 km from Addis Ababa, Ethiopia, in July 2020 by Dr. Mekonnen Abebayehu. The plant specimens were identified by Mr. Melaku Wendafrash, Addis Ababa University, Ethiopia. A voucher specimen of the plant material has been deposited in the National Herbarium, Department of Botany, Addis Ababa University, with a voucher/specimen number of MA/2007/12.

2.3. Extraction and Isolation. The collected fresh stem bark of *M. salicifolia* was air-dried at room temperature. The dried plant materials were ground using an electric grinder to obtain a fine powder. The powder (1.41 kg) was soaked and homogenized exhaustively using MeOH and $CHCl_3$ mixture at a ratio of 2 : 1. The mixture was filtered using a Buchner funnel with Whatman filter paper. The filtrates were concentrated using a rotary evaporator under reduced pressure at a temperature of 40°C. The concentrated crude extracts were allowed to dry to a constant weight at room temperature and furnished a mass of 98 g. 26.4 g of the crude extract was dissolved in chloroform and adsorbed on 25 g of silica gel, mixed well, and dried by using a rotary evaporator in order to make slurry. The sample was loaded to a glass column (55 cm × 4 cm) packed with silica gel (330 g, 70–230 mesh ASTM) and fractionated using the gradient solvent system of pet ether : $CHCl_3$ (25 : 75 to 10 : 90, v/v), $CHCl_3$: EtOAc (90 : 10 to 0 : 100, v/v), and EtOAc : MeOH (95 : 5 to 20 : 80, v/v) to give 25 fractions each 200 mL. Fractions with similar TLC profiles were combined to give twenty fractions (MS-1 to MS-20). Fraction MS-7 (5.3 g) was subjected to column chromatography over silica gel (120 g) using the gradient solvent system of pet ether : $CHCl_3$ (0 : 100 to 5 : 95, v/v) and $CHCl_3$: EtOAc (0 : 100 to 5 : 95, v/v) to give 14 subfractions, which were combined into four groups (MS-7-1 to MS-7-4) based on their TLC profile. Subfraction MS-7-1 (205.5 mg) was applied to a column chromatography packed with Sephadex LH-20 and eluted using $CHCl_3$: MeOH (1 : 1) to give compound **1** (12.4 mg). Fraction MS-9 (1.2 g) was subjected to column chromatography over silica gel (40 g) using gradient of pet ether: $CHCl_3$ (23 : 77 to 0 : 100, v/v) and $CHCl_3$: EtOAct (98 : 2 to 65 : 35, v/v) to give 10 subfractions, which were combined into three groups (MS-9-1 to MS-9-3) based on their TLC profile. Subfraction MS-9-2 (170.7 mg) was subjected to column chromatography over Sephadex LH-20 (90 g) using $CHCl_3$: MeOH (2 : 1) as eluent to give compound **2** (8.8 mg). Fraction MS-16 (2.1 g) was rechromatographed over silica gel (100 g) eluted using $CHCl_3$: EtOAc (10 : 90 to 5 : 95), followed by EtOAc : MeOH (97 : 3 to 70 : 30, v/v). Seven fractions (MS-16-1 to MS-16-7) were collected. Subfraction MS-16-4 (87 mg) was allowed to pass over Sephadex LH-20 column (90 g) eluted with $CHCl_3$: MeOH (2 : 1), and the fractionated eluents were concentrated to give compound **3** (13 mg). The subfractions MS-1 (325.5 mg) and MS-6 (102.5 mg) from pet ether : $CHCl_3$ (30 : 70, v/v) and pet ether : $CHCl_3$ (10 : 90, v/v) were dissolved in MeOH and left overnight and afforded compound **4** (10.2 mg) and compound **5** (7.6 mg), respectively. Subfraction MS-7-3 (102.5 mg) was dissolved in MeOH and left overnight; the insoluble part afforded compound **6** (42.12 mg) as a white solid. The major fraction MS-11 was concentrated and dissolved in acetone to give a precipitate named compound **7** (11.2 mg). Fraction MS-20 (1.42g) was rechromatographed over silica gel (100 g) eluted with EtOAc : MeOH mixtures (96 : 4 to 40 : 60, v/v). Five fractions (MS-20-1 to MS-20-5) were collected. Subfraction MS-20-4 (23 mg) was applied to the Sephadex LH-20 column (90 g) and eluted with $CHCl_3$: MeOH (2 : 1), and the collected fractions were concentrated to give compound **8** (5.2 mg).

2.4. Spectroscopic Data. Myricanone (**1**): a white powder; m.p. 193–195°C; IR (KBr) ν_{max} 3409.2, 2934, 2857.2, 1704.2, 1604.2, 1457.4, 1110.2, 1045.2 cm^{-1} (Figure S1); ^{1}H-NMR data: see Table 1; ^{13}C-NMR data: see Table 2; HR-*ESI*-MS *m/z* 379.15160 $[M + Na]^+$ (calc. for $C_{21}H_{24}O_5$, 379.15159).

Table 1: ^{1}H-NMR data of compounds **1**–**6** and **8**.

Position	δ_H (J in Hz)						
	1[a]	2[b]	3[a]	4[c]	5[c]	6[c]	8[d]
1	—	—		1.40, m; 1.90, m	1.63, m	1.63, m	4.19, d (7.8)
2	—	—	—	2.35, m; 2.60, m	1.59, m; 1.63, m	1.57, m; 1.62, m	3.18, d (9.6)
3	—	—		—	3.22, dt (10.6, 5.1)	3.22, dt (10.7, 5.0)	3.36, t (8.8)
4	—	—	—				3.29, m
5	—	—	—	1.34, m	0.80, m	0.80, dd (12.2, 2.5)	3.31, d (9.6)
6	—	—	—	1.57, m; 1.62, m	1.50, m; 1.63, m	1.50, m; 1.65, m	3.69, dd (11.7, 6.6); 3.89, m
7	2.56, m	2.54, ddd, (17.9, 11.4, 3.9); 2.78, m	2.46, m; 2.63, dt (17.7, 3.8)	1.04, m; 1.40, m	1.37, m; 2.06, dt (12.8, 3.3)	1.36, dd (12.9, 4.0); 2.01, dt (12.8, 3.3)	3.55, s
8	1.78, m	1.91, ddd, (13.7, 6.8, 3.8); 1.98, m	1.77, m	—	—	—	
9	1.58, m	1.50, ddt, (14.4, 10.9, 7.6; 1.68, m	1.37, dt (9.7, 4.4); 1.47, m	1.53, m	0.98, m	1.42, m	
10	2.66, t (7.2)	1.54, dd (13.6, 11.5); 1.83, ddd (13.3, 10.4, 7.3)	1.62, dd (7.9, 4.7)	—	—	—	
11	—	3.98, m	3.73, d (3.3)	1.57, m; 1.69, m;	1.44, m; 1.63, m	1.50, m; 1.64, m	
12	2.73, m	1.67, m; 2.30, ddd (15.5, 13.0, 2.8)	1.70, m; 2.12, m	1.90, ddd (13.2, 7.1, 3.3); 1.95, dd (14.7, 3.2)	1.26, m; 1.37, m	1.53, d (3.2); 1.66, m	
13	2.82, m	2.81, d (4.7); 2.91, ddd (16.3, 13.2, 2.7)	2.69, dt (16.6,3.8); 2.78, m	—	—	—	
14	—	—	—	—	—	—	
15	6.95, dd (8.2, 2.4)	7.05, dd (8.2, 2.4)	6.94, dt (5.3, 2.5)	5.58, dd (8.2, 3.2)	5.56, d (8.2, 3.2)	5.53, dd (8.2, 3.3)	
16	6.72, d (8.2)	6.8, d (8.2)	6.72, d (8.8)	1.69, m; 1.95, m	1.63, m; 1.94, dd (14.8, 3.2)	1.77, dd (15.4, 3.3); 2.14, dd (15.2,8.2)	
17	—	—	—	—	—	—	
18	6.51, d (2.5)	7.22, m	6.93, dt (5.3, 2.5)	1.01, dd (14.8, 8.1)	1.44, m	0.63, dd (13.7, 3.8)	
19	6.31, s	6.91,s	6.53, s	2.10, dt (13.0, 3.4); 1.39, m	1.00, m; 1.33, m	1.05, m; 1.43, m	
20	3.74, s	3.89, s	3.80, s	—	—	—	
21	3.76, s	3.91, s	3.78, s	1.57, m; 1.62, m	1.25, m; 1.59, m	1.29, m	
22				1.34, m; 1.39, m	1.04, m; 1.38, m	1.17, m; 1.46, m	
23				1.11, s	1.00, s	1.00, s	
24				1.01, s	0.95, s	0.82, s	
25				1.11, s	0.83, s	0.94, s	
26				0.93, s	1.11, s	1.07, s	
27				1.15, s	0.93, s	0.98, s	
28				0.85, s	0.85, s	3.16, dd (10.9, 4.8); 3.31, dd (10.9, 5.3)	
29				0.98, s	0.97, s	0.99, s	
30				0.94, s	0.93, s	0.92, s	
1′			3.98, d (7.4)				

Table 1: Continued.

Position	δ_H (J in Hz)						
	1[a]	2[b]	3[a]	4[c]	5[c]	6[c]	8[d]
2′			2.89, ddd (8.9, 7.4, 5.2)				
3′			3.05, td (8.9, 4.7)				
4′			3.21, ddt (10.2, 8.9, 5.2)				
5′			2.84, dd (11.5, 9.9); 3.49, dd (11.4, 5.3)				
11-OH		3.60 d (5.0)					
5-OH	8.85 s	8.05 s	8.87 s				
17-OH	8.70 s	7.71 s	8.62 s				

[a]Recorded in DMSO-d_6, [b]recorded in acetone-d_6, [c]recorded in $CDCl_3$, and [d]recorded in MeOD.

Table 2: ^{13}C-NMR (151 MHz) spectroscopic data for compounds (**1**–**6** and **8**).

Position	1[a]	2[b]	3[a]	4[c]	5[c]	6[c]	8[d]
1	126.9	124.8	126.5	38.4	37.7	37.7	104
2	122.8	122.7	122.9	34.1	27.2	27.1	73.7
3	148.5	146.6	148.4	217.5	79.1	79.0	76.7
4	140.4	139.4	140.3	47.6	38.9	38.8	70.2
5	149.1	148.8	149.1	55.8	55.5	55.8	76.6
6	122.3	122.9	121.8	20.0	18.8	18.8	61.4
7	27.2	25.5	25.9	35.1	41.3	41.3	55.9
8	24.5	25.8	25.4	38.9	38.8	39.1	
9	21.8	22.9	22.7	48.8	48.8	49.1	
10	45.9	39.5	35.6	35.8	38.0	37.9	
11	213.8	67.1	75.4	17.5	17.5	17.4	
12	42.4	36.7	33.3	37.7	33.1	33.4	
13	28.8	26.7	27.0	37.5	37.6	37.5	
14	131.4	130.8	130.3	157.6	158.1	159.2	
15	128.3	129.5	129.5	117.2	116.9	117.2	
16	115.9	116.2	116.2	36.7	37.7	30.8	
17	152.7	151.5	152.1	37.7	35.8	40.4	
18	133.5	133.3	134.1	48.7	49.3	44.8	
19	129.1	129.0	129.8	40.6	36.7	35.8	
20	60.5	60.8	60.5	28.8	28.8	28.6	
21	60.9	60.6	61.0	33.6	33.7	32.7	
22				33.1	35.1	27.9	
23				26.1	28.0	28.0	
24				21.5	15.5	15.4	
25				14.8	15.4	15.4	
26				29.9	25.9	26.0	
27				25.6	21.3	21.6	
28				29.9	29.8	65.5	
29				33.4	33.4	33.5	
30				21.4	29.9	29.9	
1′			101.4				
2′			73.6				
3′			77.0				
4′			70.1				
5′			66.1				

[a]Recorded in DMSO-d_6, [b]recorded in acetone-d_6, [c]recorded in $CDCl_3$, and [d]recorded in MeOD.

Myricanol (**2**): a white powder; m.p. 102–110°C; IR (KBr) ν_{max} 3369.8, 2924.2, 2855.6, 1610.8, 1585, 1502.4, 1444, 1405.2, 1352.6, 1235.8, 1059.8, 962 cm^{-1} (Figure S17); ^{1}H-NMR data: see Table 1; ^{13}C-NMR data: see Table 2; HR-ESI-MS m/z 381.16707 $[M + Na]^+$, (calc. for $C_{21}H_{26}O_5$, 381.16724).

11-O-β-D-xylopyranosylmyricanol (**3**): a white powder; m.p. 231-232°C; IR (KBr) ν_{max} 3390.8, 2927.8, 2849.6, 1501.8, 1459, 1406.2, 1347, 1229.4, 1069.2, 1039.4 cm^{-1} (Figure S26); ^{1}H-NMR data: see Table 1; ^{13}C-NMR data: see Table 2; HR-*ESI*-MS *m/z* 513.20956 $[M + H]^+$ (calc. for $C_{26}H_{34}O_9$, 513.20950).

Taraxerone (**4**): a white powder; m.p. 272–274°C; IR (KBr) ν_{max} 2928.4, 2847.8, 1709, 1474.6, 1378.6, 1153.6, 1009.6 cm^{-1} (Figure S35); ^{1}H-NMR data: see Table 1; ^{13}C-NMR data: see Table 2; MALDI-MS (positive-ion mode) *m/z* 449.9 $[M + Na + H]^{2+}$ (calc. for $[C_{30}H_{48}ONaH]^{2+}$, 449.7).

Taraxerol (**5**): a white powder; m.p. 257–260°C; IR (KBr) ν_{max} 3430.8, 3051.4, 2929, 2860.4, 1751.2, 1620, 1449.2, 1385.8, 1081.4 cm^{-1} (Figure S44); ^{1}H-NMR data: see Table 1; ^{13}C-NMR data: see Table 2; MALDI-MS (positive-ion mode) *m/z* 449.9 $[M + Na]^+$ (calc. for $[C_{30}H_{50}ONa]^+$, 449.73).

Myricadiol (**6**): a white powder; m.p. 266–268°C; IR (KBr) ν_{max} 3392, 2936, 2855, 1644.4, 1461.2, 1382, 1018.2 cm^{-1} (Figure S53); ^{1}H-NMR data: see Table 1; ^{13}C-NMR data: see Table 2; MALDI-MS (positive-ion mode) *m/z* 442.1 $[M]^+$ (calc. for $C_{30}H_{50}O_2$, 442.7).

3β-O-trans-caffeoylisomyricadiol (7): a white powder; m.p. 292–294°C; IR (KBr) ν_{max} 3434.2, 2937.8, 2868.4, 1695.6, 1616.6, 1526.4, 1471, 1389.8, 1278.6, 1221.6, 1159.2, 1001.8, 808 cm^{-1} (Figure S62); ^{1}H-NMR data: see Table 3; ^{13}C-NMR data: see Table 3; MALDI-MS *m/z* 897.8 as $[M + (DHB\text{-}H_2O)_2 + Na\text{-}2H]^+$ (calc. for $C_{39}H_{56}O_5$, 897.0).

Methyl-β-D-glucopyranose (**8**): a colorless crystal; m.p. 104–106°C; IR (KBr) ν_{max} 3420, 2928.2, 2858.6, 1643.8, 1454.8, 1071, 1027 cm^{-1} (Figure S70); ^{1}H-NMR data: see Table 1; ^{13}C-NMR data: see Table 2; HR-*ESI*-MS *m/z* 217.06848 $[M + H]^+$ (calc. for $C_7H_{14}O_6$, 217.06826).

2.5. Antioxidant Activity Assays by 2, 2-Diphenyl-1-Picrylhydrazyl (DPPH). The antioxidant activities of the isolated compounds were assessed using DPPH radical scavenging activity with ascorbic acid as the positive control as per the previously described method [16]. All extracted compounds were separately dissolved in DMSO (1 mg/mL) and serially diluted with methanol, followed by addition of 0.004% (4 mg/100 mL) methanolic solution of DPPH to get 3.12, 6.25, 12.5, 25, and 50 μg/mL, and the absorbance of each dilution, after 30 minutes, was measured at 517 nm. An ascorbic acid solution of the same concentration (3.12 μg/mL to 50 μg/mL) was prepared in similar fashion and measured.

The DPPH radical scavenging activity of each of the tested compounds was reported as percentage inhibition using the following formula:

$$\%\ \text{DPPH Inhibition} = \left[\frac{A_{\text{control}} - B_{\text{sample}}}{A\ \text{control}}\right] \times 100, \quad (1)$$

where *A* control is the absorbance of DPPH solution and *B* sample is the absorbance of the test sample (DPPH solution plus compound).

The DPPH solution was used as a negative control. The relative half-maximal inhibitory concentration (IC_{50}) values were calculated using the plotted % RSA and double-verified using trusted online computational tools [17]. The final antioxidant activity of each compound was expressed as the IC_{50} value.

2.6. Antibacterial Activity. The four common standard ATCC strains, *Staphylococcus aureus* (*S. aureus*, ATCC 25923), *Escherichia coli* (*E. coli*, ATCC 25922), Streptococcus pyogenes (*S. pyogenes*, ATCC 19615), and *Pseudomonas aeruginosa* (*P. aeruginosa*, ATCC 27853) were obtained from Adama Science and Technology University (ASTU).

Table 3: ^{1}H (600 MHz), ^{13}C (151 MHz, DMSO-d_6), HMBC (600 MHz), and COSY (600 MHz) NMR spectroscopic data of compounds **7**.

Position	δ_c	δ_H	COSY	HMBC	C atom	δ_c	δ_H	COSY	HMBC
1	37.3	1.00 (H_1) 1.56 (H_2)	H_2-2 H_2-2	C-2, 3, 10 C-5, 10, 25	21	32.9	1.17 (H_1) 1.24 (H_2)	H_1-22 H_2-22	C-20 C-17, 22, 20, 21, 30, 29
2	23.7	1.58 (H_1) 1.63 (H_2)	H_1-1 H_1-1	C-1, 3, 4, 10 C-1, 3, 4, 10	22	27.8	1.00 (H_1) 1.49 (H_2)	H_2-21 H_2-21	C-21 C-20
3	80.2	4.49 (dd, J = 11.7, 4.5 Hz)	H_2-2	C-2, 4, 5, 23, 24, 9′	23	28.2	0.84		C-3, 4, 5, 24
4	37.9				24	17.1	0.92		C-3, 4
5	55.5	0.92	H_2-6	C-3, 6, 7, 9, 24, 25	25	15.6	0.94		C-1, 5, 9
6	18.7	1.49 (H_1) 1.58 (H_2)	H-5	C-4, 5, 7 C-4, 5, 7	26	26.3	1.04		C-7, 9, 14
7	41.3	1.31 (H_1) 1.99 (H_2)	H_2-6 H_1-7	C-9, 26 C-5, 8, 9, 26	27	21.8	0.933		C-13, 14
8	38.9	—			28	63.5	2.89 (H_1) 3.00 (H_2)	H_2-28 H_1-28	C-16, 17 C-16, 17, 22
9	48.9	1.44	H_2-11	C-5, 11, 25, 26	29	33.9	0.95		C-20, 21
10	37.8				30	30.2	0.87		C-19, 20, 21, 29
11	17.4	1.46 (H_1) 1.61 (H_2)	H_1-12	C-9, 12, 13 C-8, 9, 13,	1′	115.2	7.04 (d, J = 2.1 Hz, 1H)		C-2′, 3′, 5′, 7′
12	33.6	1.47 (H_1) 1.61 (H_2)	H_1-11	C-9, 11, 13, 14, 27 C-9, 11, 13, 14, 27	2′	146.2	—		
13	37.4	—			3′	148.8	—		
14	158.0				4′	116.2	6.76 (d, J = 8.1 Hz, 1H-4′)	H-5′	C-2′, 3′, 5′, 6′
15	116.4	δ 5.58 (dd, J = 8.2, 3.2 Hz)	H_2-16	C-8, 13, 16, 17	5′	121.7	7.00 (dd, J = 8.2, 2.1 Hz, 1H),	H-4′	C-1′, 3′, 7′
16	30.6	1.56 (H_1) 2.12 (dd, J = 14.8, 8.1 Hz) (H_2)	H-15	C-14, 15, 28 C-14, 15, 17, 18, 28	6′	125.9	—		
17	40.5	—			7′	145.2	7.45 (d, J = 15.8 Hz)	H-8′	C-1′, 6′, 8′
18	45.0	0.47 (dd, J = 13.6, 3.6 Hz)	H_1-19 H_2-19	C-13, 17, 19	8′	114.9	6.24 (d, J = 15.9 Hz)	H-7′	C-6′, 9′
19	36.0	1.00 (H_1) 1.37 (H_2)		C-18, 20, 30 C-18, 20, 30	9′	166.8	—		
20	28.8								

Experiments were conducted in close consultation with the Microbiology Laboratory of the Applied Biology Department of ASTU.

The *in-vitro* antibacterial susceptibility test was determined by the disc diffusion method [18]. The medium was prepared by dissolving 38 g of Mueller–Hinton agar in 1000 mL of distilled water in 2.5 L flask. The flask was placed on a hot plate with a magnetic stirrer, and the mixture was heated slowly until the powder was completely dissolved and then autoclaved at 121°C for 15 min. The autoclaved medium was poured into sterile Petri dishes (20 mL/plate), and the plates were allowed to solidify under sterile conditions at room temperature. Then, the plates were seeded with an overnight grown culture approximately 1.5×10^8 CFU/mL by swabbing evenly on the surface of the medium with a sterile cotton swab.

The isolated compounds at concentrations of 250 μg/mL and 500 μg/mL were prepared by dissolving in 10% 10% aqueous DMSO [19, 20]. 6.0 mm in diameter discs made of Whatman filter paper No. 1 were infused with the solutions of the isolated compounds and placed on the surface of the medium by gently pressing down to ensure contact with the MHA. Plates were inverted and incubated at 37°C for 24 hours. Ampicillin was used as a standard antibiotic positive control [21], while 10% aqueous DMSO was used as a negative control. After incubation, the inhibition zones were evaluated by measuring the diameter (mm) of the clear zone around the discs. All the experiments were performed in triplicate and interpreted using the CLSI zone diameter interpretative standards [18] and compared with 10 μg/mL controls.

2.7. Computational Methods

2.7.1. Molecular Docking. The interaction and binding affinity of the isolated compounds was investigated against PqsA protein of *P. aeruginosa* (PDB: 50E4), pyruvate kinase (PK) enzyme of *S. aureus* (PDB: 3T07), LuxS protein of *S. pyogenes* (PDB: 1INN), and DNA gyrase of *E. coli* (PDB: 6F86). The crystal structures of the proteins were downloaded from the protein data bank and processed by removing the cocrystallized ligands, deleting water molecules, and adding polar hydrogen and cofactors according to the AutoDock 4.2.6 (MGL tools 1.5.7) procedure [22]. After cleaning the proteins, only polar hydrogens and the Kollman charges were introduced. Nonpolar hydrogen atoms were merged, and Gasteiger partial atomic charges were assigned. In line with the experiment, we used ampicillin as a standard control drug. The grid center coordinates were 70, 70, and 70 pointing in the x, y, and z directions, respectively, with a grid point spacing of 0.375 Å. The center grid box was 9.393, −0.025, and 13.018 Å. 50 different conformations were generated for each targeted isolated compound. Furthermore, to gain deeper insights into the biological activities of the isolated compounds, we conducted a comparative analysis with the binding interactions of ciprofloxacin against the aforementioned proteins. This comparative assessment aims to provide a comprehensive understanding of the potential activities exhibited by the isolated compounds in comparison to the well-known antibacterial agent ciprofloxacin. The conformation of the compounds with the lowest binding free energy was selected to analyze the interactions with the receptors using the Discovery Studio Visualizer.

2.7.2. In-Silico Prediction of the Pharmacokinetics and Physicochemical Properties. Swiss ADME [23], an online prediction tool, was used to predict the pharmacokinetics of the isolated compounds. Parameters such as lipophilicity, molecular weight, water solubility, hydrogen bond donors and acceptors, bioavailability score, gastrointestinal absorption, and blood-brain barrier permeability were computed [23]. The OSIRIS property explorer and ProTox online server [24] were used to determine the oral toxicity and LD_{50} values of the investigated compounds.

3. Results and Discussion

3.1. Structure Elucidation of Isolated Compounds. The chloroform-methanol (2 : 1) extract of the stem bark of *M. salicifolia* was subjected to column chromatography to afford eight compounds **1**–**8** (Figure 1). Three diarylheptanoids were isolated and characterized as myricanone (**1**) [25], myricanol (**2**) [25], and myricanol-11-O-β-D-xylopyranoside (**3**) [26]. Four triterpenoids, taraxerone (**4**) [27], taraxerol (**5**) [28], myricadiol (**6**) [29], and 3β-*O*-*trans*-caffeoylisomyricadiol (**7**), were isolated. One pyranoside, methyl-β-D-glucopyranoside (**8**), was also isolated and characterized [30, 31]. This is the first report of compounds **4**, **5**, **6**, **7**, and **8** from *M. salicifolia*.

Compound **1** was isolated as a white powder with the melting point of 193–195°C. The IR spectrum (Figure S8) revealed a broad absorption band centered at 3369.8 cm^{-1} due to O-H stretching vibration, 2924.2 cm^{-1} and 2855.6 cm^{-1} due to C-H stretching vibration, 1704.2 cm^{-1} due to C=O stretching of aliphatic ketone, 1614.8 cm^{-1} and 1585.0 cm^{-1} due to C=C stretching vibrations, 1110.2 cm^{-1}–1045 cm^{-1} due to C-O, and 750 cm^{-1}–1000 cm^{-1} due to the aromatic CH group. The molecular formula was established as $C_{21}H_{24}O_5$ by the sodiated-molecular-ion peak in the HR-*ESI*-MS at m/z 379.1516 $[M + Na]^+$ (calcd for $C_{21}H_{24}O_5Na$, 379.1516) (Figure S7). The ^{1}H-NMR spectrum (Figure S1) of the aromatic region confirmed the presence of four aromatic protons, with a singlet at δ_H 6.31 (H-19) and three mutually coupled protons at δ_H 6.95 (H-15), 6.72 (H-16), and 6.51 (H-18), indicating the presence of one proton in one aromatic ring and three in 1,2,4-relative positions in the other aromatic ring. In addition, the observed four oxygenated aromatic carbons at δ_C 140.4 (C-4), 148.5 (C-3), and 149.1 (C-5) supported the hypothesis that one of the aromatic rings has the pyrogallol oxidation pattern. Three aromatic proton signals were observed as an ABX system at 6.95 (dd, $J = 8.2$, 2.4 Hz, H-15), 6.72 (d, $J = 8.2$ Hz, H-16), and 6.51 (d, $J = 2.5$ Hz, H-18) in the ^{1}H-NMR spectra (Table 1). The presence of two methoxy groups was deduced from the ^{1}H-NMR spectra at δ_H 3.76 (3H-21) and 3.74 (3H-20) and

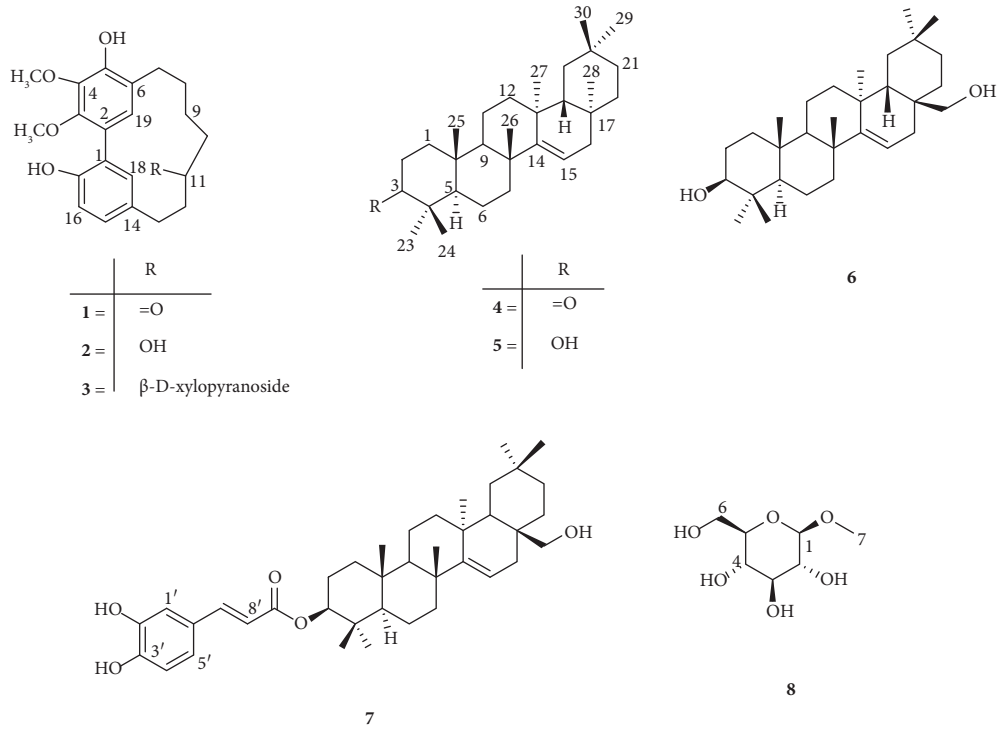

Figure 1: Chemical structures of the isolated compounds.

the ^{13}C-NMR spectra at δ_C 60.9 (C-21) and 60.5 (C-20). The HMBC showed a correlation between the deshielded methoxyl groups (δ_H 3.74 (H-20) and δ_H 3.76 (H-21)) and the aromatic carbons at δ_C C-148.5 (C-3) and C-140.3 (C-4), respectively, indicative of a di-*ortho*-substitution. The ^{13}C-NMR, DEPT, and HSQC spectra (Figures S2, S3, and S5) revealed 21 carbon atoms corresponding to two methyls, six methylenes, four methines, and eight quaternary carbon signals, as well as the typical peaks of a carbonyl carbon and twelve aromatic carbons (Table 2). In the HMBC spectrum (Figure S6), OH-protons at δ_H 8.87 and δ_H 8.62 are attached to C-5 (δ_C 149.1) and C-17 (δ_C 152.7), respectively, thus supporting the attachment of OH-to the phenol ring. In the ^{1}H-NMR, the two hydroxy groups were resonating highly down field at δ 8.85 (s, OH-5) and 8.70 (s, OH-17) than expected because when a five, six, and seven-membered conjugated ring and the π-delocalization of the hydrogen bonded heteroconjugated fragment result in a resonance-assisted with an intramolecular hydrogen bond in the compound structure, δOH resonance in DMSO-d6 is more deshielded, i.e., the hydrogen bond is stronger than the expected aromatic systems [32]. The COSY spectra (Figure S4) showed correlations of protons H-7/H-8/H-9/H-10 and H-12/H-13. Six methylene carbons at δ_C 45.9 (C-10), 42.4 (C-12), 28.8 (C-13), 27.2 (C-7), 24.5 (C-8), and 21.8 (C-9) and one carbonyl carbon at δ_C 213.8 (C-11) were also identified and linked together in a chain, as demonstrated by the absence of a carbon resonance associated with a point of branching. The HMBC correlations of the methylene protons H-9, H-10, H-12, and H-13 with C-11 revealed that C-10 and C-12 are connected through a C=O group at the 11-position, while HMBC correlations between δ_C 2.56 (H-7) and 149.1 (C-5), 122.3 (C-6), 129.1 (C-19), and between δ_H 2.82 (H-13), 128.3 (C-15), and 131.4 (C-14) were used to link the aliphatic chain with the diphenyl moiety, and consequently compound **1** was determined as myricanone (Figure 1) by comparison of these data (Tables 1 and 2) and the literature data [25].

Compound **2** was isolated as an amorphous white powder with a melting point of 102–110°C. The IR spectra (Figure S17) of compound **2** revealed a broad absorption band at 3369.8 cm^{-1} due to O-H stretching vibration, 2924.2 cm^{-1} and 2855.6 cm^{-1} due to C-H stretching vibration of the aliphatic chain, and 1610.8 cm^{-1}–1444.0 cm^{-1} due to C=C stretching vibrations of aromatic. Its molecular formula, $C_{21}H_{26}O_5$, was determined from HR-*ESI*-MS at *m/z* 381.1670 $[M+Na]^+$ (calcd for $C_{21}H_{26}O_5Na$, 381.1672) (Figure S16). The ^{1}H-and DEPT-NMR spectrum (Figures S9 and S11) of compound **2** was very similar to that of **1**, except the aliphatic side chain contains OH at C-11. This observation was supported by a methine proton at δ_H 3.98 bonded to C-11 (δ_C 67.1). Furthermore, methane proton signal at δ_H 3.98 showed HMBC correlations with C-10 and C-12. Its ^{13}C-NMR spectra (Figure S10 and Table 2) were similar to those of compound **1**, except for position 11. In contrast, the carbonyl group at C-11 (δ_C 213.8) in **1** was replaced by a hydroxyl group (δ_C 67.1). The ^{1}H and ^{13}C-NMR values for all the protons and carbons were assigned on the basis of 2D-NMR (Figure S12–S15) correlations and were given in Tables 1 and 2. As a result, compound **2** was identified as myricanol by comparison of these data found in the literature [25].

Compound **3** was isolated as an amorphous white powder with a melting point of 231-232°C. The IR (Figure S26) of compound **3** revealed a broad absorption band at 3390.8 cm^{-1} due to O-H stretching vibration, absorptions at 2927.8 cm^{-1} and 2849.6 cm^{-1} due to C-H stretching, 1501.8 cm^{-1}–1406.2 cm^{-1} due to C=C stretching vibration of aromatics, and 1352.6 cm^{-1} and 1235.8 cm^{-1} due to C-O-C stretching vibrations of aromatic methoxy. The molecular formula was established to be $C_{26}H_{34}O_9$ from HR-*ESI*-MS at *m/z* 513.2095 $[M+Na]^+$ (calcd for $C_{26}H_{34}O_9Na$, 513.2095) (Figure S25). The ^1H and ^{13}C-NMR data of compound **3** (Tables 1 and 2) were similar to those of compound **2**, except for an additional sugar moiety at C-11. The anomeric proton and carbon of the sugar moiety resonated at δ_H 3.98 (d, $J = 7.4$ Hz, H-1′) and δ_C 101.4 (C-1′) in the ^1H, ^{13}C-NMR, and DEPT spectra (Figures S18–S20), respectively. The remaining sugar carbons characteristic of D-xylose appeared at δ_C 66.1 (5′), 70.1 (C-4′), 73.6 (C-2′), and 77.0 (C-3′) [33]. The relative configuration of the xylose sugar moiety was also assigned by ^1H-^1H coupling constants, HSQC, and NOESY correlations (Figures S21, S22 and S24). H-1′ (δ_H 3.98) and H-2′ (δ_H 2.89) were located at axial positions which were confirmed by the large coupling constant value of ^{3}JH1′-H2′ (7.4 Hz). The coupling constant of 8.9 Hz between H-2′ (δ_H 2.89) and H-3′ (δ_H 3.05) also indicated their axial-axial relationship. The large coupling value (8.9 Hz) between H-3′ and H-4′ revealed that H-3′ (δ_H 3.05) and H-4′ (δ_H 3.21) are located on the axial positions of the sugar. Furthermore, the NOESY correlations of H-1′ (δ_H 3.98) and H-3′ (δ_H 3.05) assigned that these two protons are found in the same plane, while H-2′ (δ_H 2.89) and H-4′ (δ_H 3.21) protons are found on the other side, so that the OH at H-3′ is *trans* to H-2′ and H-4′. If two adjacent hydrogen atoms in a six-membered ring are *trans* (i.e., diaxial), a value of 7–10 Hz should be observed for JH-H, while only 2–4 Hz should be observed if the hydrogen atoms are gauche (i.e., axial-equatorial) [34]. The attachment of the sugar moiety at C-11 was supported by the HMBC (Figure S23) correlation between the anomeric proton at δ_H 3.98 (H-1′) and C-11 (δ_C 75.4). Hence, based on the above data (Tables 1 and 2) and comparison with the literature data, compound **3** was proposed to be 11-*O*-*β*-D-xylopyranosylmyricanol [26].

Compound **4** was isolated as a white powder with a melting point of 272–274°C. The infrared spectrum (Figure S35) of compound **4** revealed absorptions at 3051.4 cm^{-1} due to = C-H stretching vibration and absorptions at 2929.0 cm^{-1} and 2860.4 cm^{-1} due to C-H stretching vibration of alkanes. The sharp peaks appeared at 1709 cm^{-1} due to the C=O stretching vibration of carbonyl groups and at 1474 cm^{-1} and 1378.6 cm^{-1} due to C=C stretching vibrations and umbrella mode of $-CH_3$ symmetric bending, respectively. Its molecular formula was deduced to be $C_{30}H_{48}O$ by the MALDI-MS (Figure S34) from the molecular ion peak at *m/z* 449.9 for $[M+Na+H]^{2+}$ (calc. for $[C_{30}H_{48}ONaH]^{2+}$, 449.7). ^1H-NMR, ^{13}C, and DEPT spectra (Figures S27–S29) showed eight singlet methyl signals at chemical shifts of δ_H 1.15 (H-27), 1.12 (H-25), 1.11 (H-23), 1.01 (H-24), 0.98 (H-29), 0.94 (H-30), 0.93 (H-26), and 0.85 (H-28), which were associated with the relevant carbon resonances at δ_C 33.4 (C-29), 29.9 (C-26), 29.8 (C-28), 26.1 (C-23), 25.6 (C-27), 21.5 (C-24), 21.4 (C-30), and 14.8 (C-25), suggesting the presence of a pentacyclic triterpenoid structure [27]. There were four methine protons, the double ($J = 8.2$, 3.2 Hz) centered at δ_H 5.58 (H-15) is attributable to the olefinic proton at C-15. A multiplet at δ_H 1.34 (m), multiplet at δ_H 1.53 (m), and a doublet of doublet at δ_H 1.01 (14.8, 8.1) are attributable to the methine protons at C-5, C-9, and C-18, respectively. ^1H-NMR and ^{13}C spectrum showed ten methylene signals at chemical shifts of δ_H 1.40 (m, H_1-1), 1.90 (m, H_2-1), 2.35 (m, H_1-2), 2.60 (m, H_2-2), 1.57 (m, H_1-6), 1.62 (m, H_2-6), 1.04 (m, H_1-7), 1.40 (m, H_2-7), 1.57 (m, H_1-11), 1.69 (m, H_2-11), 1.00 (d, $J = 3.7$ Hz, H_1-12), 1.34 (m, H_2-12), 1.69 (m, H_1-16), 1.95 (m, H_2-16), 2.10 (dt, $J = 13.0$, 3.4, H_1-19), 1.39 (m, H_2-19), 1.57 (m, H_1-21), 1.62 (m, H_2-21), 1.34 (m, H_1-22), and 1.39 (m, H_2-22). ^{13}C-NMR and DEPT spectra showed 30 carbon signals: eight methyls, ten methylenes, four methines, and four quaternary carbons, of which one of the quaternary carbons at δ_C 217.5 (C-3) was a carbonyl carbon. The COSY spectrum (Figure S30) of compound 4 showed correlations between H-1 and H-2, H-6 and H-7, H-15 and H-16, H-21 and H_2-22, H-9 and H-11, H-5 and H_2-6, and H-18 and H-19, which are characteristics of the connectivity sequence in the pentacyclic ring. In HSQC spectra, protons correlate with their directly attached carbon which is shown in Figure S31. The olefin was attributed to C-14 based on long-range HMBC (Figure S32) correlations of the methyl singlets H-26 and H-27 with C-14 and H-16 with C-14. NOESY (Figure S33) correlations showed that H-24/H-25, H-26/H-18, and H-30/H-26/H-28 were found on the same side of the molecule, whereas H-23/H-5, H-5/H-9, and H9/H-27 were found on the opposite side of the molecule. Therefore, the structure of compound **4** was determined to be taraxerone [27].

Compound **5** was isolated as a white powder with a melting point of 257–260°C. Its IR spectrum (Figure S44) at 3430.8 cm^{-1} was due to O-H stretching vibration, 3051.4 cm^{-1} due to = C-H stretching vibration, and 1620 cm^{-1} due to C=C stretching vibrations. Its molecular formula was deduced to be $C_{30}H_{50}O$ using the MALDI-MS at *m/z* 449.9 $[M+Na]^+$ (calc. for $C_{30}H_{50}ONa$, 449.7) (Figure S43). Its NMR (Figures S36–S38) spectroscopic data were identical to those of **4**, except for the absence of carbonyl carbon signals in **5**, which was replaced by an OH group at C-3. This was confirmed by the shielded chemical shift of C-3 at δ_C 79.1 and the COSY (Figure S39) correlation δ_H 3.22 (H-3) with H-2. In HSQC spectrum, protons correlate with their directly attached carbon which is showed in Figure S40. The HMBC (Figure S41) correlations of methyl protons H-23 and H-24 with C-3 also supported the assignment. The relative configuration of OH was determined to be 3*β* from the NOESY (Figure S42) correlations of H-3 and H-5. Therefore, the structure of compound **5** was elucidated as taraxerol [28].

Compound **6** was isolated as a white amorphous powder with a melting point of 266–268°C. Its molecular formula was deduced to be $C_{30}H_{50}O_2$ from the MALDI-MS at *m/z* 442.1 $[M]^+$ (calc. for $C_{30}H_{50}O_2$, 442.7) (Figure S52). Its spectroscopic data (Figures S45–S49) were identical to those

of compound **5**, except for the presence of a hydroxylated carbon signal at δ_C 65.5 (C-28) in the ^{13}C-NMR spectrum of compound **6**. The presence of this additional hydroxyl group was confirmed by the ^{1}H-NMR signal for diastereotopic protons at δ_H 3.16 and 3.31 (H-28), as shown by the HMBC (Figure S50) correlations with C-17, C-22, and C-16. NOESY (Figure S51) correlations showed that H-24/H-25/H-26 and H-18/H-28/H-30 were all classified as β-oriented due to their appearances on the same side of the molecule. Whereas, the H-3/H-23/H-5, H-5/H-9, and H9/H-27 NOESY correlations showed that they were α-configured. Based on the spectroscopic data (Tables 1 and 2) and comparison with the literature data, compound **6** was determined to be myricadiol [29].

Compound **7** was obtained as a white amorphous powder with a melting point of 292–294°C. The molecular formula was found to be $C_{39}H_{56}O_5$, via the MALDI-MS (Figure S61) with *m/z* 897.8 for $[M + (DHB\text{-}H_2O)_2 + Na\text{-}2H]^+$ (calc. for $C_{39}H_{56}O_5$, 897.0). The ^{1}H, ^{13}C-NMR, and DEPT spectra (Figures S54–S56) of compounds **7** (Table 3) and **6** were nearly superimposable for the pentacyclic moiety. Differences were observed due to the signals of a *trans*-caffeoyl moiety in **7**. This group was identified in the ^{1}H-NMR from two olefinic *trans* coupled protons at δ_H 7.45 (d, $J = 15.8$ Hz, H-7′) and 6.24 (d, $J = 15.9$ Hz, H-8′) and three aromatic protons at δ_H 6.76 (d, $J = 8.1$ Hz, H-4′), 7.00 (dd, $J = 8.2$, 2.1 Hz, H-5′), and 7.04 (d, $J = 2.1$ Hz, H-1′); the coupling relationship established a 1,3,4-substituted benzene ring [35]. The attachment of the caffeoyl group at C-3 via an ester linkage was deduced from the HMBC (Figure S59) correlation of H-3 (δ_H 4.49) with caffeoyl group carbonyl carbon C-9′ (δ_C 166.8). The relative configuration of the stereogenic center of **7** was deduced from the ^{1}H-^{1}H coupling constant (Figure S57) and the NOESY (Figure S60) experiment. The typical coupling constant for H-3 ($J = 11.7$, 4.5 Hz) in the ^{1}H-NMR spectrum revealed that H-3 was in the α-orientation. The difference in the multiplicity with a larger coupling constant of H-3 in **7** was in agreement with the respective coupling patterns (axial-equatorial and axial-axial) of H-3 and H_2-2, indicating that H-3 is situated in an axial position [36, 37]. In the HSQC spectrum, protons correlate with their directly attached carbon that is shown in Figure S58. In addition, α-orientation of H-3, H-5, H-9, H-23, and H-27 was suggested by the NOESY interactions of H-3 to H-23/H-5 and H-9 to H-5/H-23/H-27. Thus, the structure of compound **7** was determined to be 3β-(3′, 4′-dihydroxy-*trans*-cinnamoyloxy)-D-friedoolean-14-en-3α, 28-diol and named with a trivial name 3β-*O*-*trans*-caffeoylisomyricadiol.

Compound **8** was isolated as a colorless crystal with a melting point of 104–106°C. A strong broad IR (Figure S70) absorption band characteristic of the bonded-OH group was observed at 3420 cm^{-1}, absorptions at 2928.2 cm^{-1} and 2858.6 cm^{-1} due to C-H stretching vibration of CH_3, CH_2, and CH. The molecular formula was established as $C_7H_{14}O_6$ by an *ESI*-MS (Figure S69) at *m/z* 217.06848 $[M + Na]^+$ (calcd for $C_7H_{14}O_6$, 217.06826). Seven carbon atoms were identified by the ^{13}C-NMR and DEPT spectra, indicating a sugar moiety. A detailed analysis of 1D and 2D NMR spectra (Figures S63–S68 and Tables 1 and 2) and comparison with the literature indicated that the results were in line with those for methyl-β-D-glucopyranoside. The pyranose moiety′s ^{13}C-NMR values were consistent with those seen in the literature [31].

3.2. Antioxidant Activity. The antioxidant capacities of the isolated compounds, expressed as the DPPH free radical inhibition and the IC_{50} values, are presented in Table 4.

According to antioxidant activity parameters, the IC50 value category is very strong if the IC50 value is <10 μg/mL, strong if the IC50 value is between 10 and 50 μg/mL, mild if the IC50 value is between 50 and 100 μg/mL, weak if the IC50 value is between 100 and 250 μg/mL, and not active if IC50 is above 250 μg/m [38]. The relative IC_{50} values for the isolated compounds were in the range of 13.48 μM–740.83 μM (Table 4). Compound **2** ($IC_{50} = 13.48\,\mu$M) showed the highest antioxidant activity compared to other isolated compounds, while compound **8** ($IC_{50} = 740.83\,\mu$M) showed the lowest antioxidant activity. The IC_{50} values recorded for diarylheptanoid compounds **1**, **2**, and **3** were 19.55 μM, 13.48 μM, and 97.99 μM, respectively, whereas 282.61 μM, 306.32 μM, 59.31 μM, and 23.95 μM were reported for compounds **4**, **5**, **6**, and **7**, respectively. In diarylheptanoid compounds, the most susceptible OH group is the phenolic *hydroxyl* group, which confirms the importance of the enolic-OH moiety for the highest antioxidant activity of compound **2**. The presence of the ketone functional group in compound **1** and the sugar moiety in compound **3** might be responsible for their reduced antioxidant activity in comparison to compound **2**. The attached sugar moiety creates steric hindrance in compound **3**, which may reduce its antioxidant activity compared to compound **6** [39, 40]. Of the tri*terpenoid* compounds, compound **7** has a phenylpropanoid moiety, which increases its antioxidant activity compared to other *terpenes*. This suggests that the phenylpropanoid moiety is an essential functional group for the observed antioxidant activity.

3.3. Antibacterial Activity. The *in-vitro* antibacterial activities of compounds 1–7 against Gram-positive (*S. aureus* and *S. pyogenes*) and Gram-negative (*E. coli* and *P. aeruginosa*) bacterial strains were examined at doses of 250 μg/mL and 500 μg/mL compared with 10 μg/mL of positive controls. The measured inhibition zones of the compounds are presented in Table 5.

The inhibition zone for the seven isolated compounds against *E. coli* ranges from 6.5 to 9.5 mm at a concentration of 250 μg/mL. The compound having better activity against *E. coli* was compound **3** (inhibition zone of 9.0 mm) compared to other isolated compounds. Compounds **3** (10.0 mm) and **7** (10.0 mm) displayed the highest activity against *S. pyogenes*, while compound **4** showed the lowest inhibition zone (7.0 mm) against *S. aureus*, followed by compounds **6** (8.5 mm) and **7** (9.0 mm). Against the Gram-negative bacteria *P. aeruginosa*, the highest activity was recorded for compound **3** (8.5 mm), followed by compound **7** (8.0 mm) at a concentration of 250 μg/mL. The results of the present study generally indicate that compounds **3** and **7**

Table 4: Percent radical scavenging activity and IC_{50} values of the isolated compounds.

Cpds	% DPPH inhibition at					r^2	IC_{50} (μM)
	50 μg/mL	25 μg/mL	12.5 μg/mL	6.25 μg/mL	3.12 μg/mL		
1	79.59	68.98	58.91	46.59	35.59	0.99	19.55
2	88.86	86.68	79.06	67.45	52.74	0.93	13.48
3	82.10	76.92	67.30	57.33	45.30	0.98	97.99
4	35.71	26.73	24.13	22.26	20.85	0.84	282.61
5	31.78	27.33	24.91	23.14	21.65	0.95	306.32
6	52.22	41.74	31.26	25.57	22.54	0.95	59.31
7	96.23	87.32	46.23	24.15	13.88	0.95	23.95
8	33.69	27.36	24.21	22.28	20.59	0.92	740.83
Ascorbic acid	97.32	97.27	97.25	97.19	96.96	0.81	2.07

Note. r^2: coefficient of determination; IC_{50}: half maximal inhibitory concentration.

Table 5: Antibacterial activities of isolated compounds.

Bactria strains	Gram-positive bacteria				Gram-negative bacteria			
Conc. (μg/mL)	*S. pyogenes*		*S. aureus*		*P. aeruginosa*		*E. coli*	
	250	500	250	500	250	500	250	500
1	8.0	9.0	7.5	8.5	7.0	8.0	7.0	8.0
2	9.0	10.5	8.5	10.0	8.0	9.0	8.0	9.0
3	10.0	11.5	9.0	10.5	8.5	10	9.0	11.0
4	7.5	8.0	7.0	7.5	6.5	7.0	6.5	7.5
5	8.0	9.0	8.0	8.5	7.0	8.0	7.0	8.0
6	9.0	10.0	8.5	9.0	7.5	8.5	8.0	9.0
7	10.0	11.0	9.0	10.0	8.0	9.0	8.5	10.0
Amp	14.0	—	13.0	—	12.5	—	13.0	—
Cipro. [41][a]	20.79	—	21.72	—	20.90	—	21.54	—

Note. **1**–**7**: compounds, Amp: ampicillin (+ve control), Conc: concentration, Cipro: ciprofloxacin. [a]The concentration of ciprofloxacin is 200 μg/ml.

displayed better activities to inhibit the growth of both Gram-positive and Gram-negative bacterial strains compared to other compounds, and the lowest activity was exhibited by compound **4**. All the isolated compounds showed relatively weaker activities compared to the standard drugs ampicillin and ciprofloxacin. However, compared to the growth of Gram-negative bacteria, it was more effective against the growth of Gram-positive bacteria. Several studies suggest that the antibacterial activity of polyphenols is generally more effective against Gram-positive than Gram-negative bacteria due to cell walls linked to a molecularly complex outer membrane that slows down the passage of chemicals [42].

The results from this study suggest that the higher antibacterial and antioxidant activity of compounds **3** and **7** could be attributed to the complex phenolic compounds. In the case of compound **3** with the skeletal structure of two aromatic rings linked together with seven carbon chains and possesses strong nucleophilic properties, which may allow it to donate an electron pair to electrophilic functional groups of plasma membrane proteins and/or lipids, probably leading to membrane dysfunction [43]. For the activity displayed by compound **7**, the presence of caffeoyl group might be responsible. This seems to be in line with our findings that showed better antibacterial performance of compounds **3** and **7** than the other compounds.

3.4. Computational Study

3.4.1. Molecular Docking Investigation. The *in silico* molecular docking study of the isolated compounds (**2**, **3,** and **7**) against PqsA protein of *P. aeruginosa*, pyruvate kinase (PK) enzyme of *S. aureus*, LuxS protein of *S. pyogenes*, and DNA gyrase of *E. coli* are discussed. The three isolated compounds **2**, **3,** and **7** interacted (Figures 2 and 3) with the main amino acids of pyruvate kinase of *S. aureus* (PDB: 3T07 and have minimum binding energy ranging from −6.95 to −10.05 kcal/mol, with the best result achieved for compound **7** (−10.05 kcal/mol)) (Table 6) compared to the standard drugs ampicillin and ciprofloxacin, and it has good interaction affinities with the residual amino acids (Figure 4 and 5). Compound **7** has a stronger binding energy with the lowest inhibition constant (K_i) 0.04 μM than the standard drugs since it interacts through four hydrogen bonds between residues Met1, Asn29, Asp58, and Arg443 with the oxygen of hydroxyl and oxygen of ketone of the isolated compounds (Figure 6). On the other hand, the hydrogen bond interaction of ampicillin and ciprofloxacin was with Asn29, Lys59, Ile60, Pro418 and Met1, Asp58, and Lys59 (Figures 4 and 5), respectively. Moreover, hydrophobic (π-Sigma/π-Alkyl) and van der Waals interactions between compound **7** and residues Glu60, Pro118, Gly65, Pro79, Gly119, and Glu124 were observed, which are different from the standard drug.

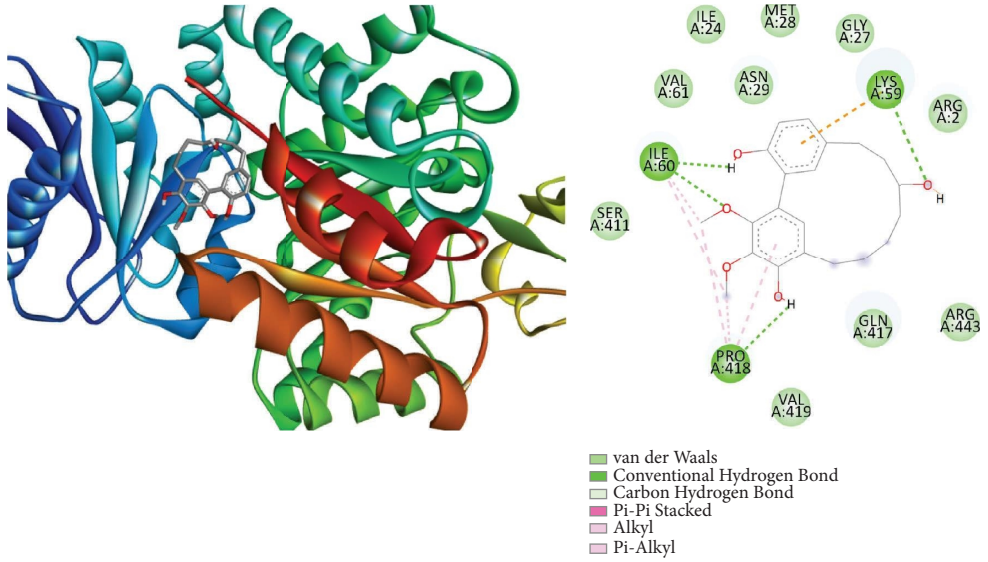

Figure 2: The binding interactions of **2** against pyruvate kinase of *S. aureus* (PDB: 3T07).

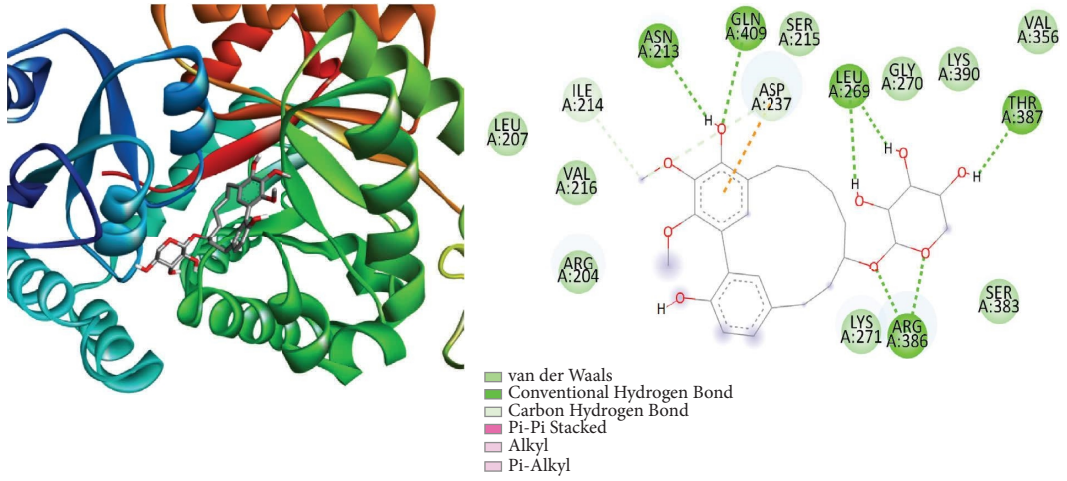

Figure 3: The binding interactions of **3** against pyruvate kinase of *S. aureus* (PDB: 3T07).

The three isolated compounds **2**, **3,** and **7** interacted (Figures 7–9) with the main amino acids of pqsA of *p. aeruginosa* (PDB: 50E4) and have minimum binding energy ranging from −7.35 to −10.35 kcal/mol, with the best result achieved for compound **7** (−10.35 kcal/mol) (Table 6), with the lowest inhibition constant (K_i) 0.03 μM than ampicillin and ciprofloxacin since it interacts through different hydrophobic and van der Waals interactions. But hydrogen bond with Tyr163 for compound **7** showed less binding scores compared to ampicillin and ciprofloxacin which interacts through four hydrogen bonds: Thr164, Asp382, Arg372, Arg397 and Thr164, Thr304, Arg372, Arg397 (Figures 10 and 11), respectively. The three isolated compounds **2**, **3,** and **7** interacted (Figures 12–14) with the main amino acids of LuxS of *S. pyogenes* (PDB: 1INN) and have minimum binding energy ranging from −5.51 to −7.45 kcal/mol, with the best result achieved for compound **7** (−7.45 kcal/mol) (Table 7). It also showed hydrophobic/π-cation interactions with Glu60 and Pro118 of a phenyl and methyl groups of the compound, respectively. On the other hand, Gly65, Pro79, Gly119, and Glu124 showed van der Waals residual interactions (Figure 14), while ampicillin and ciprofloxacin form H-bonds with Asp76, Ser78, and Gly81 and Asp76, respectively, and hydrophobic and van der Waals interactions with various amino acid residues at the active sites are presented (Figures 15 and 16).

The isolated compounds **2**, **3**, and **7** interacted with the main amino acid residues of the DNA gyrase of *E. coli* (PDB: 6F86) through H-bonds, van der Waals, and π-sigma/π-alkyl (hydrophobic) interactions (Figures 17–19). Compound **7** forms H-bonds with Val71, and hydrophobic and van der Waals interactions with various amino acid residues at the active sites are presented in Table 7 and Figure 19, while ampicillin and ciprofloxacin form H-bonds with Asn46 and Asp73, and Asp49, Gly77, and Arg136, respectively, and hydrophobic and van der Waals interactions with various

Table 6: Molecular docking scores and the corresponding prominent residual amino acid interactions of the isolated compounds and standard drugs ampicillin and ciprofloxacin against *S. aureus* and *p. aeruginosa*.

Compounds	Lowest binding energy (kcal/mol)	Inhibition constant (K_i)	H-bonding with	π-Sigma/π-alkyl	van der Waals
Against pyruvate kinase of S. aureus (PDB: 3T07)					
2	−6.95	8.01 μM	Lys59, Ile60, Prof418	—	Asn29, Val61, Gln417
3	−6.90	8.73 μM	Asn213, Leu269, Arg386, Gln409	—	Ile214, Asp237, Lys271, Ser383
7	−10.05	0.04 μM	Met1, Asn29, Asp58, Arg443	Arg2, Ile60, Ile398, Val419	Lys59, Gln417, Pro418, Thr441
Ampicillin	−7.36	4.04 µM	Asn29, Lys59, Ile60, Pro418	Val420	Lys55, Gln417, Val419
Ciprofloxacin	−6.83	9.79 μM	Met1, Asp58, Lys59	Ile398, Arg443	Arg2, Ile60, Gln417, Thr441
Against pqsA of p. aeruginosa (PDB: 50E4)					
2	−7.35	4.08 μM	Thr163, Gly210, Thr304	Phe208, Phe209	Thr164, Thr211
3	−8.07	1.21 μM	Pro234	Trp233	Ile204, Pro205, Val254, Ile257
7	−10.35	0.03 μM	Tyr163	Ile83, Phe208, Phe209, Trp233	Val82, Asn84, Lys206, Pro234
Ampicillin	−8.03	1.30 µM	Thr164, Asp382, Arg372, Arg397	—	Lys172, Ile301, Glu305, Thr380
Ciprofloxacin	−6.54	16.17 μM	Thr164, Thr304, Arg372, Arg397	Ile301, Ala303, Glu305, Tyr378	Ala278, Gly279, Gly381, Asp382

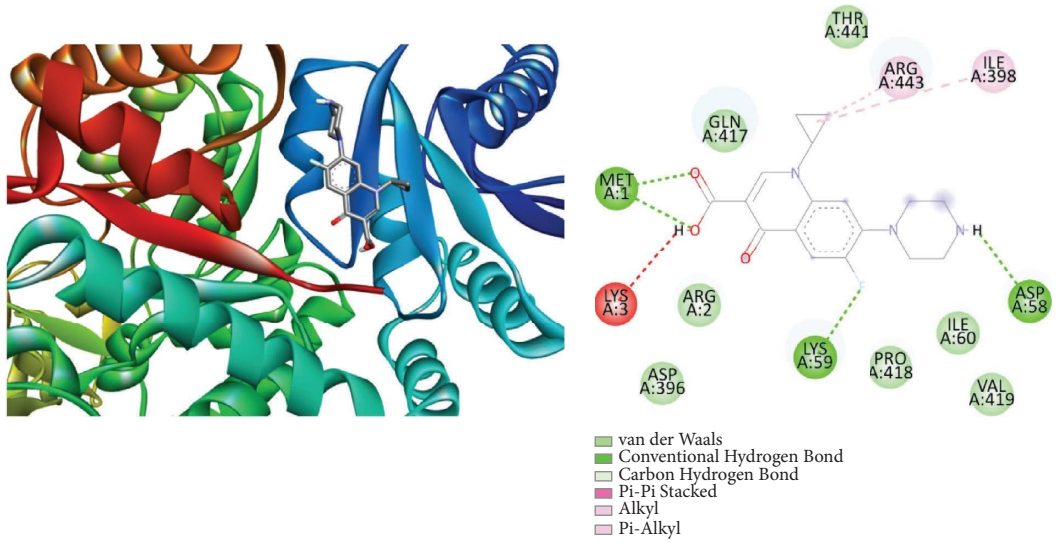

Figure 4: The binding interactions of ciprofloxacin against pyruvate kinase of *S. aureus* (PDB: 3T07).

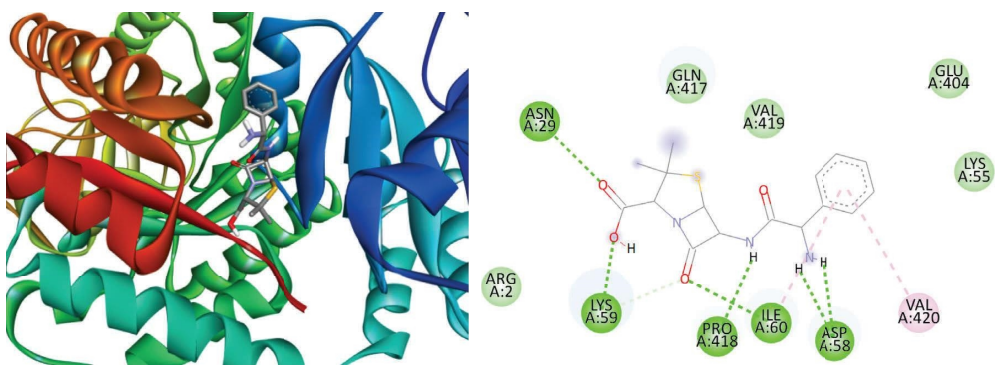

Figure 5: The binding interactions of ampicillin against pyruvate kinase of *S. aureus* (PDB: 3T07).

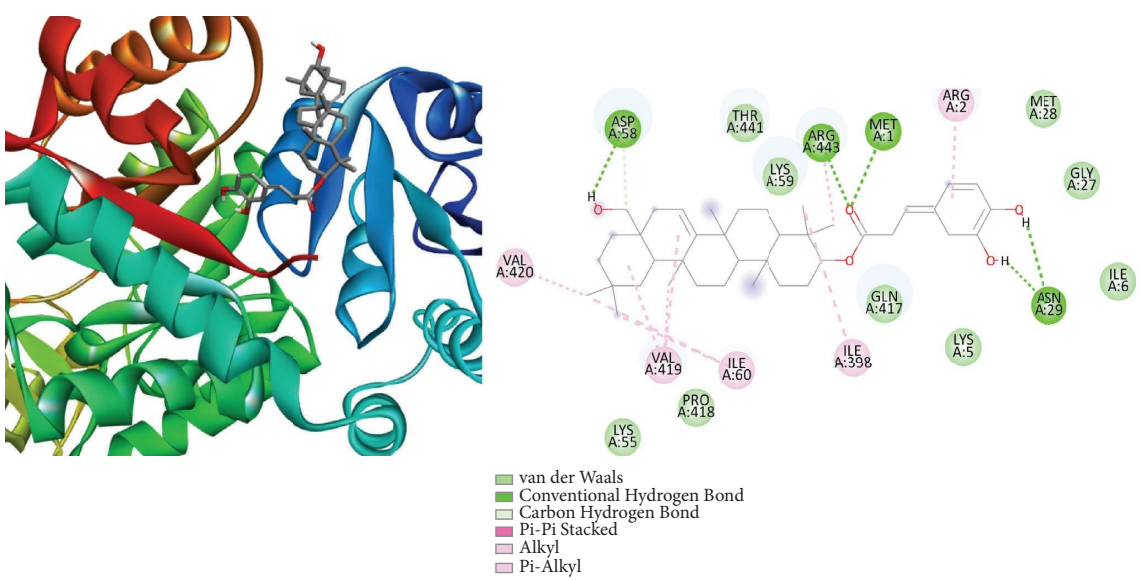

Figure 6: The binding interactions of **7** against pyruvate kinase of *S. aureus* (PDB: 3T07).

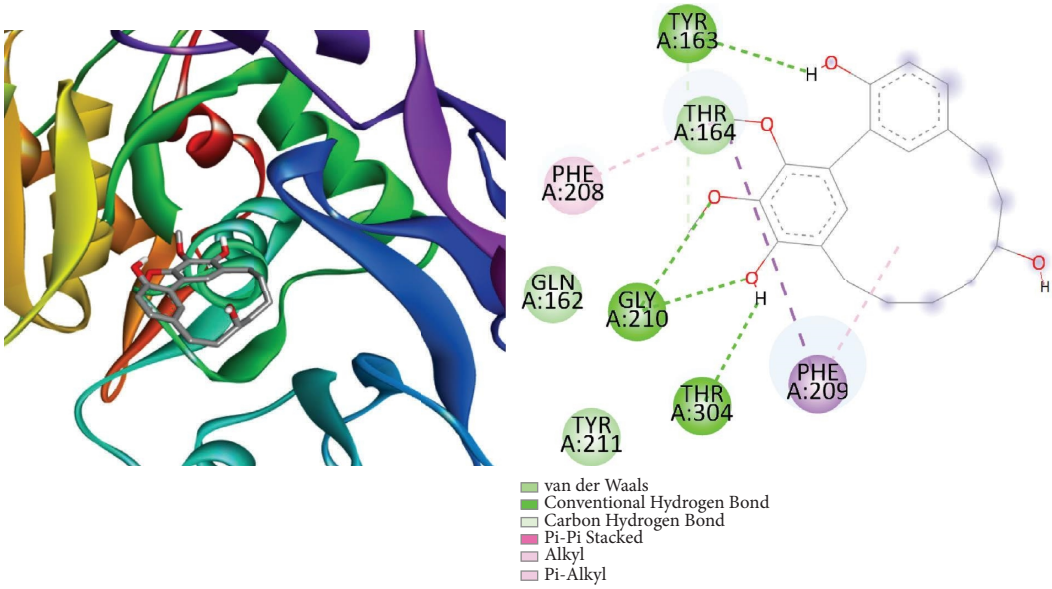

Figure 7: The binding interactions of **2** against pqsA of *p. aeruginosa* (PDB: 50E4).

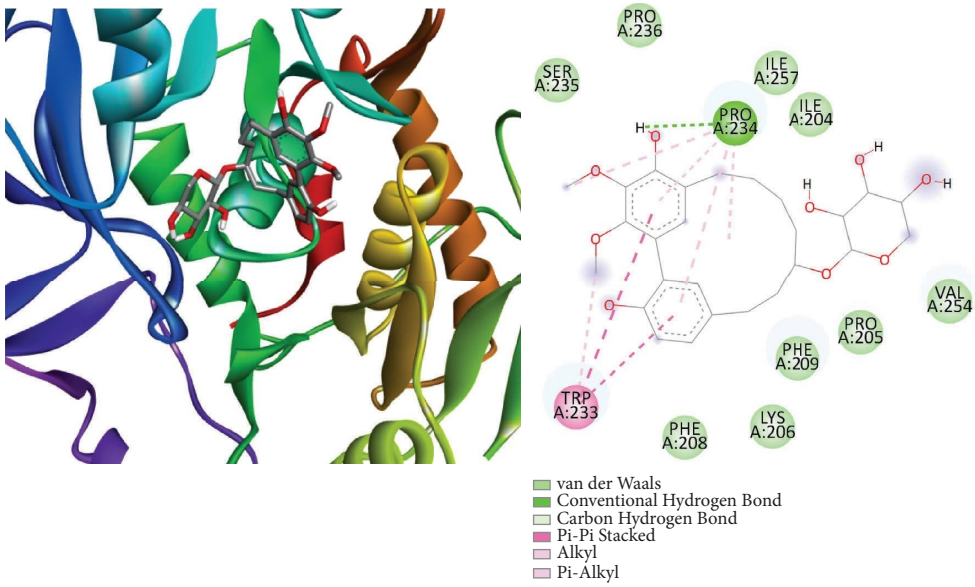

Figure 8: The binding interactions of **3** against pqsA of *p. aeruginosa* (PDB: 50E4).

amino acid residues at the active sites are presented in Figures 20 and 21. The binding scores range from −6.27 to −9.72 kcal/mol with the best binding energy achieved for compound **7** with −6.72 kcal/mol and inhibition constant (K_i) 0.07 μM, while for ampicillin and ciprofloxacin, the binding energies were −7.52 kcal/mol and −6.19 kcal/mol and inhibition constants (K_i) were 3.07 μM and 28.85 μM, respectively. The significant binding interaction of compound **7** with the target proteins could suggest possible activity of these isolated compounds against *S. aureus*, *p. aeruginosa S. pyogenes,* and *E. coli.* Interestingly, the standard exhibits higher antibacterial activity despite having a lower binding energy than compound **7**. This divergence in antibacterial activity could be attributed to specific interactions crucial for the antibacterial efficacy, potentially linked to the complete solubility of the isolated compounds. To understand the precise nature of interactions between the compounds and the target proteins, further investigations are imperative. A more in-depth analysis, especially *in-vivo* bioassay study, is required to discern the factors contributing to the observed variations in antibacterial activity, ensuring a comprehensive understanding of the underlying mechanisms at play. As preliminary evidence, the two-dimensional interactions projections make it clear that, in comparison to the two compounds, the standard exhibits a significantly higher number of specific hydrogen bond interactions with the target protein residues which might be linked to its activity. A similar situation was encountered in the work of

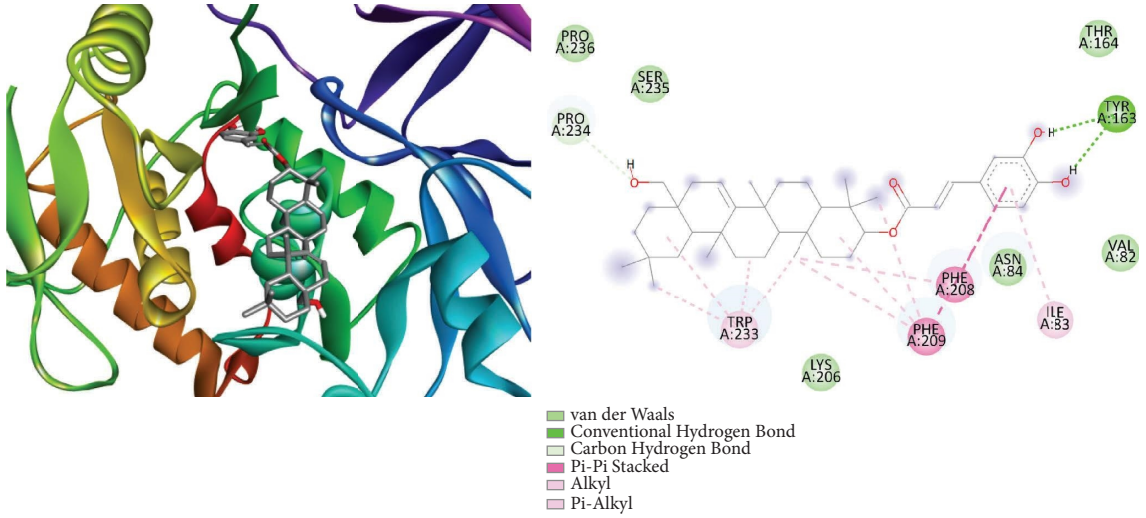

Figure 9: The binding interactions of **7** against pqsA of *p. aeruginosa* (PDB: 50E4).

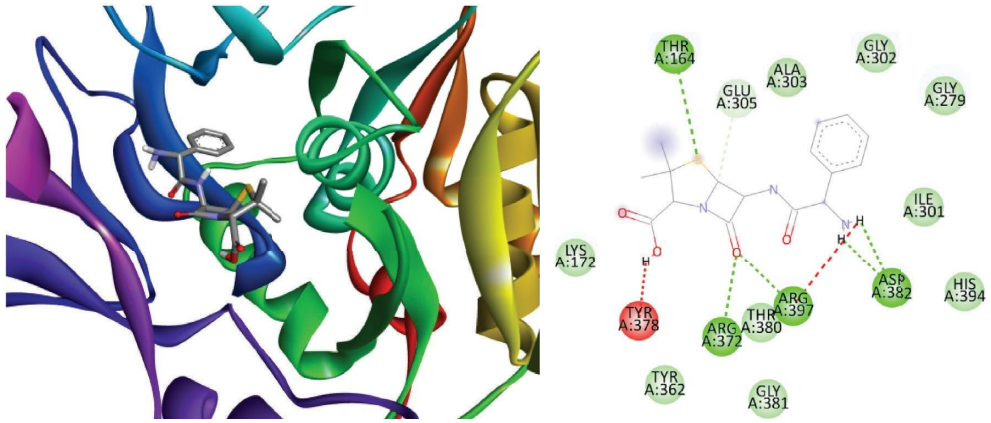

Figure 10: The binding interactions of ampicillin against pqsA of *p. aeruginosa* (PDB: 50E4).

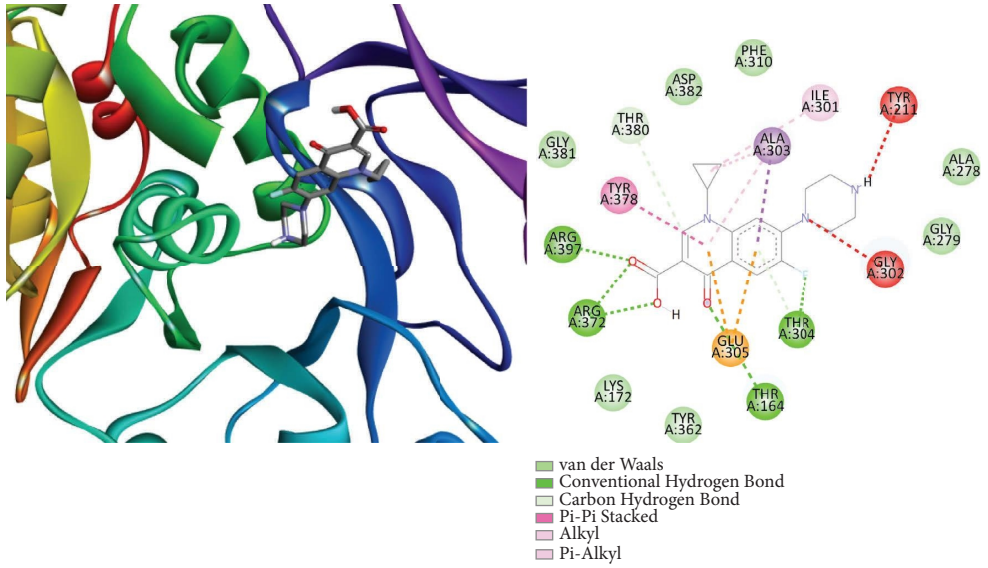

Figure 11: The binding interactions of ciprofloxacin against pqsA of *p. aeruginosa* (PDB: 50E4).

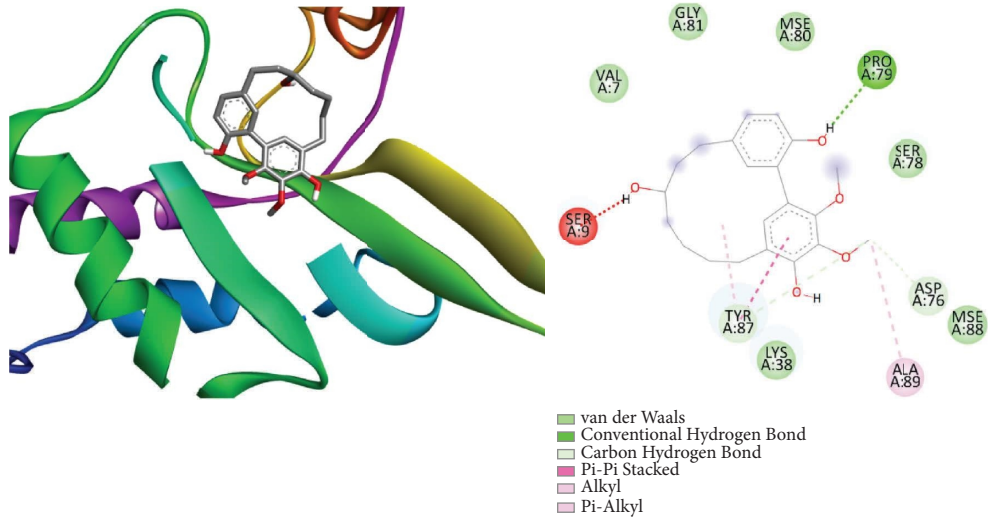

Figure 12: The binding interactions of **2** against LuxS of *S. pyogenes* (PDB: 1INN).

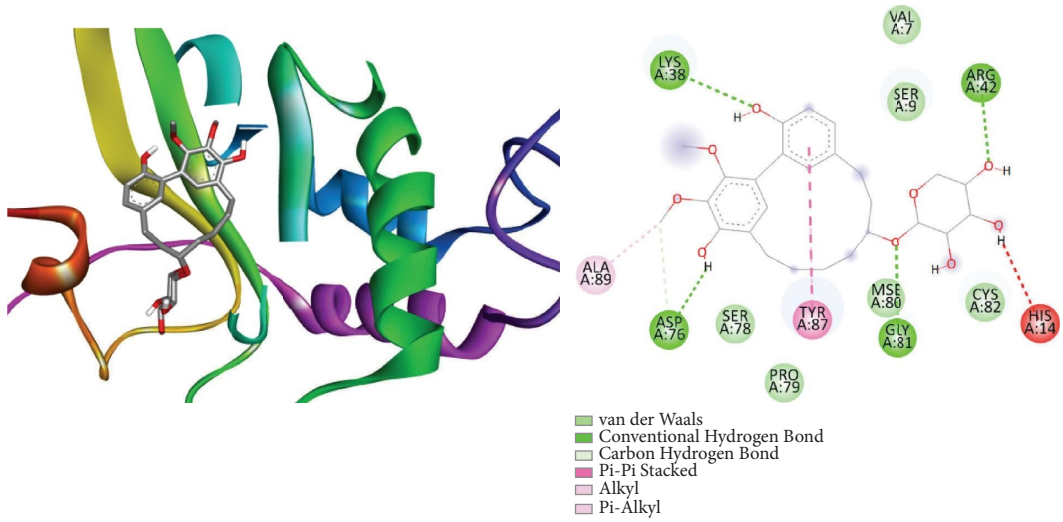

Figure 13: The binding interactions of **3** against LuxS of *S. pyogenes* (PDB: 1INN).

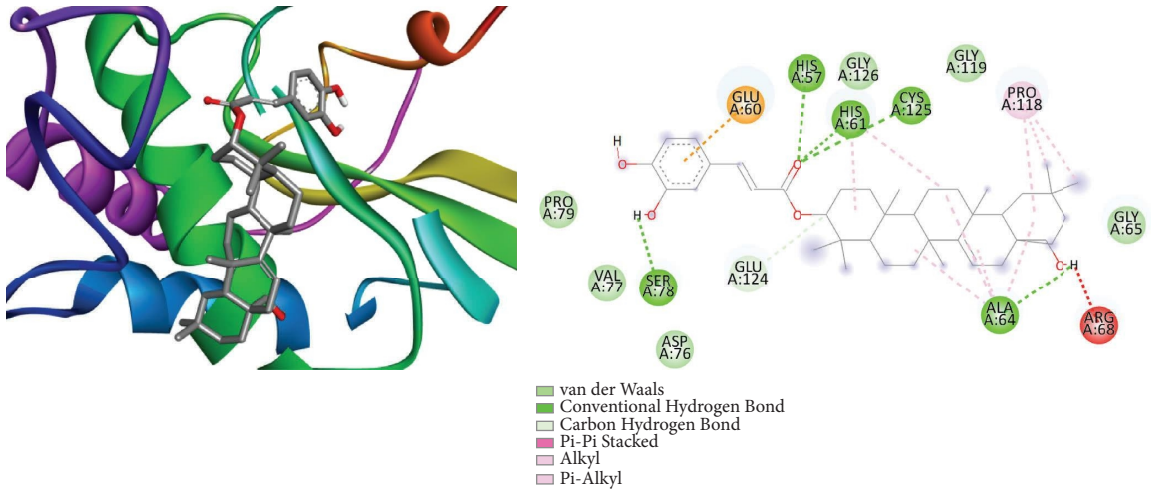

Figure 14: The binding interactions of **7** against LuxS of *S. pyogenes* (PDB: 1INN).

Table 7: Molecular docking scores and the corresponding prominent residual amino acid interactions of the isolated compounds and standard drugs ampicillin and ciprofloxacin against *S. pyogenes* and *E. coli*.

Compounds	Lowest binding energy (kcal/mol)	Inhibition constant (K_i)	H-bonding with	π-Sigma/π-alkyl	van der Waals
Against LuxS of S. pyogenes (PDB: 1INN)					
2	−5.51	90.77 μM	Pro79	Ala89	Lys38, Asp76, Tyr87, Mse88
3	−6.07	35.73 μM	Lys38, Arg42, Asp76, Gly81	Tyr87,Ala89	Ser9, Mse80, Cys82, Ser78
7	−7.45	3.43 μM	His57, His61, Ala64, Cys125	Glu60, Pro118	Gly65, Pro79, Gly119, Glu124
Ampicillin	−7.26	4.79 µM	Asp76, Ser78, Gly81	Lys38, Tyr87, Ala89	Pro79, Mse80, Cys82, Mse88
Ciprofloxacin	−5.86	50.54 μM	Asp76	Ala25, Lys38, Mse88, Ala89	Ser9, Arg23, Ser78, Tyr87
Against DNA gyrase of E. coli (PDB: 6F86)					
2	−6.27	25.54 μM	Asn46, Arg76, Gly77	Glu50, Ile78	Asp73, Pro79, Arg136, Thr165
3	−6.65	13.39 μM	His64, Ser70, Asp73, Gln135	Ile60, Met166	Asp74, Lys162, Lys162, Arg168
7	−9.72	0.07 μM	Val71	Val43, Ile78, Ile94, Thr165	Glu50, Asp73, Val120, Met166
Ampicillin	−7.52	3.07 μM	Asn46, Asp73	Val43, Ala47, Arg76, Val167	Glu50, Gly77, Ile78, Thr165
Ciprofloxacin	−6.19	28.85 μM	Asp49, Gly77, Arg136	Glu50, Arg76, Ile78, Pro79	Asn46, Thr165

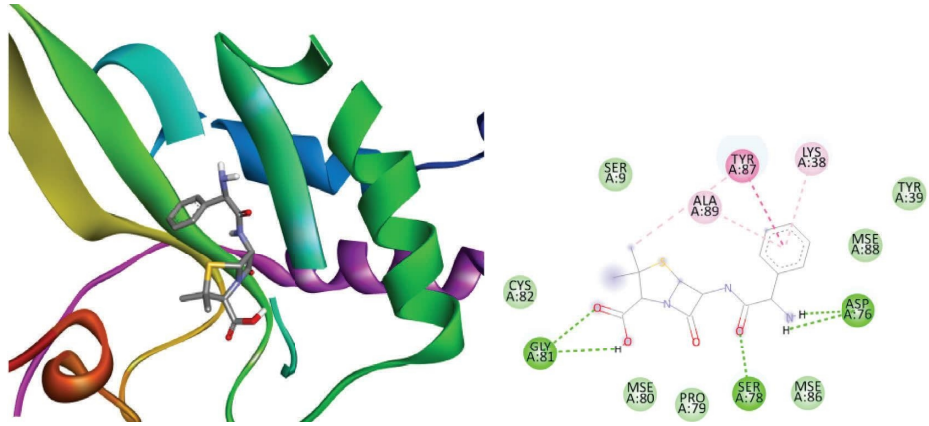

Figure 15: The binding interactions of ampicillin against LuxS of *S. pyogenes* (PDB: 1INN).

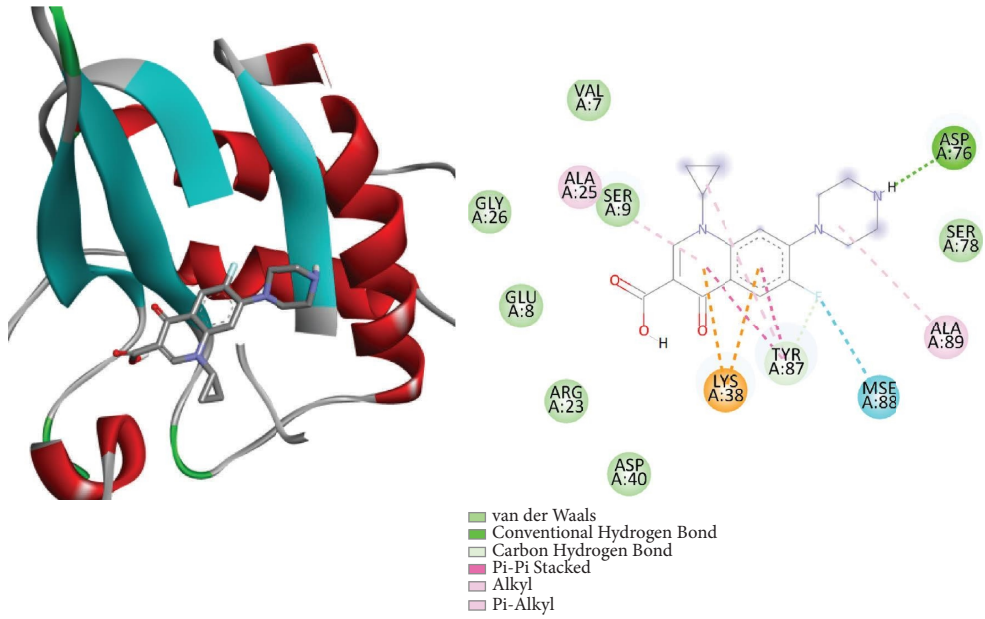

Figure 16: The binding interactions of ciprofloxacin against LuxS of *S. pyogenes* (PDB: 1INN).

[44, 45] where good antibacterial and antitubercular activities of isolated compounds and ligands are observed as a result of specific interactions with important protein residues despite smaller binding energies.

3.4.2. In Silico Pharmacokinetics and Toxicity Analysis. The drug-likeness of the isolated compounds was characterized according to "Lipinski's rule of five." As per Lipinski's rule, the potential compounds should have the following physicochemical properties [46], such as (i) total polar surface area (TPSA), which should not be >140 Å; (ii) a number of hydrogen bond donors ≤5, number of hydrogen bond acceptors ≤10; (iv) a molecular mass ≤500 Da; and (v) log *P* not ≥5. The Swiss ADME-computed results (Table 8) showed that compounds **1**–**3** and **8** in the present study satisfy Lipinski's rule of five with zero violations [47]. Except for compound **7**, all the studied compounds recorded a lipophilicity (iLogP) value of less than five (range from 1.25 to 4.77), indicating their optimal lipophilicities for good oral and intestinal absorption. Compounds **1**–**3**, **4**–**7**, and **8** presented log S values of −4.47 to −4.84, −7.50 to −9.57, and 0.76, respectively. The drug-likeness of the isolated compounds was characterized according to "Lipinski's rule of five." As per Lipinski's rule, the potential compounds should have the following physicochemical properties [46], such as (i) total polar surface area (TPSA) which should not be >140 Å, (ii) a number of hydrogen bond donors ≤5, number of hydrogen bond acceptors ≤10, (iv) a molecular mass ≤500 Da, and (v) log *P* not ≥5. The Swiss ADME-computed results (Table 8) showed that compounds **1**–**3** and **8** in the present study are satisfying Lipinski's rule of five with zero violations [47]. Except for compound **7**, all the studied compounds recorded a lipophilicity (iLogP) value of less than five (range from 1.25 to 4.77), indicating their optimal lipophilicities for good oral and intestinal absorption.

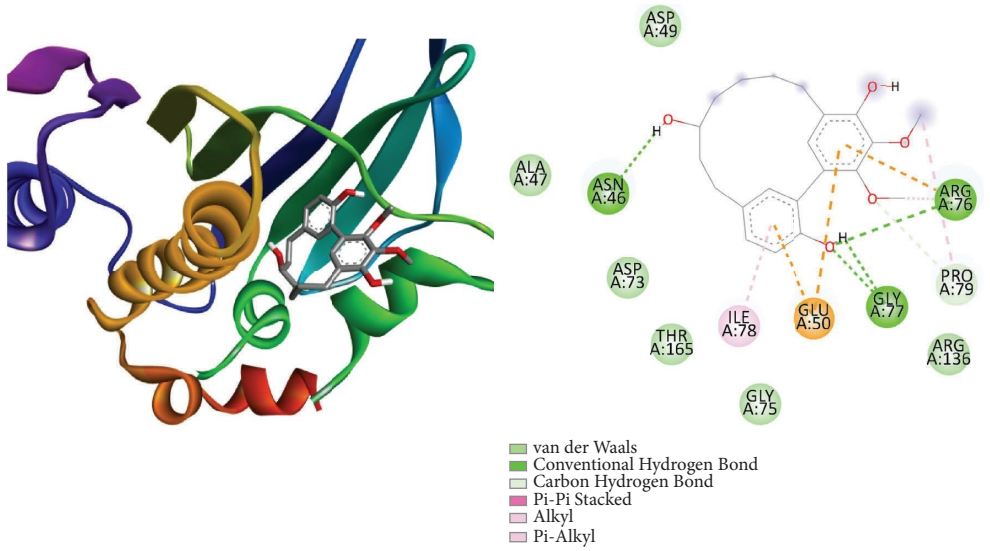

Figure 17: The binding interactions of **2** against DNA gyrase of *E. coli* (PDB: 6F86).

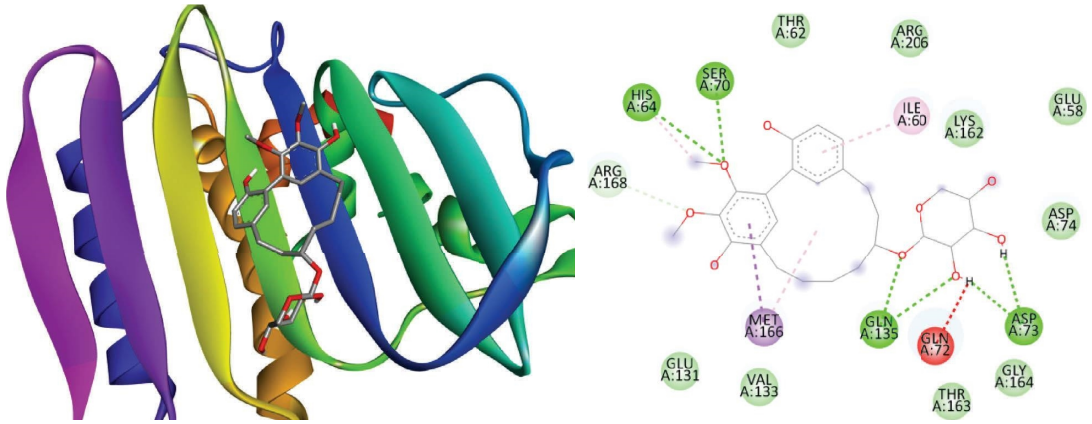

Figure 18: The binding interactions of **3** against DNA gyrase of *E. coli* (PDB: 6F86).

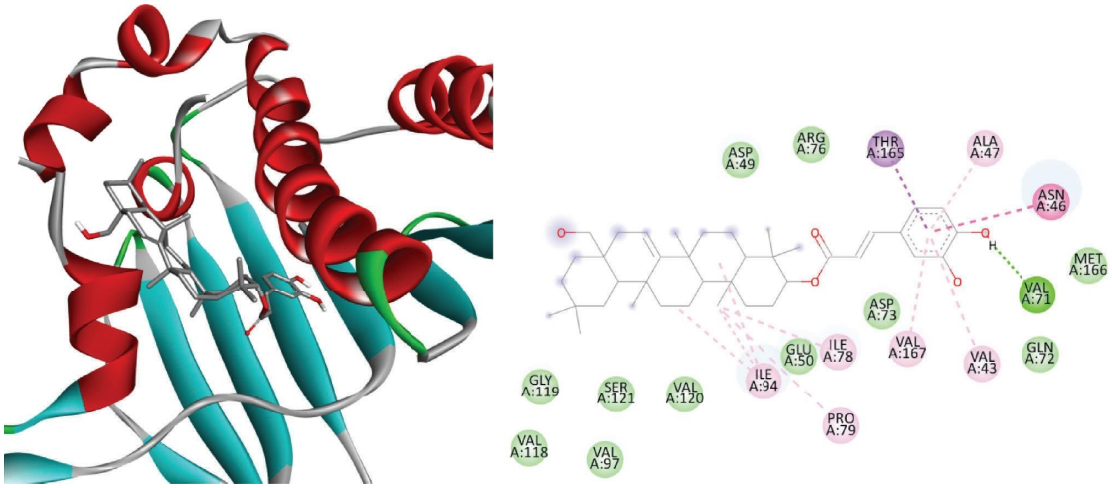

Figure 19: The binding interactions of **7** against DNA gyrase of *E. coli* (PDB: 6F86).

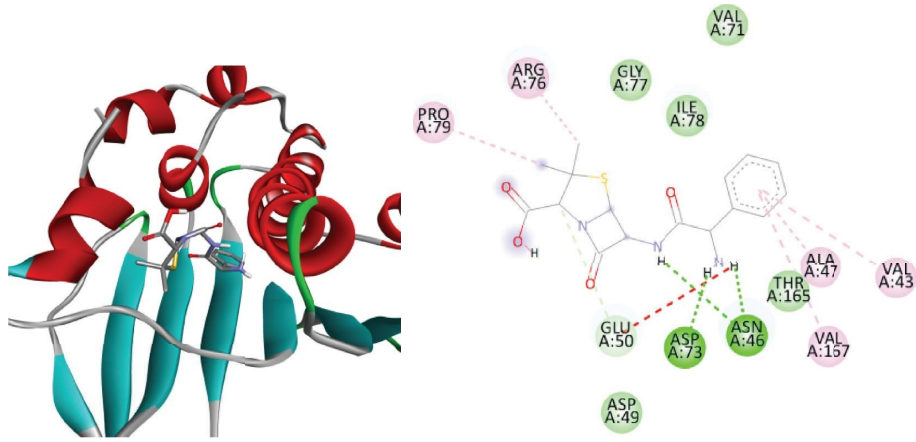

Figure 20: The binding interactions of ampicillin against DNA gyrase of *E. coli* (PDB: 6F86).

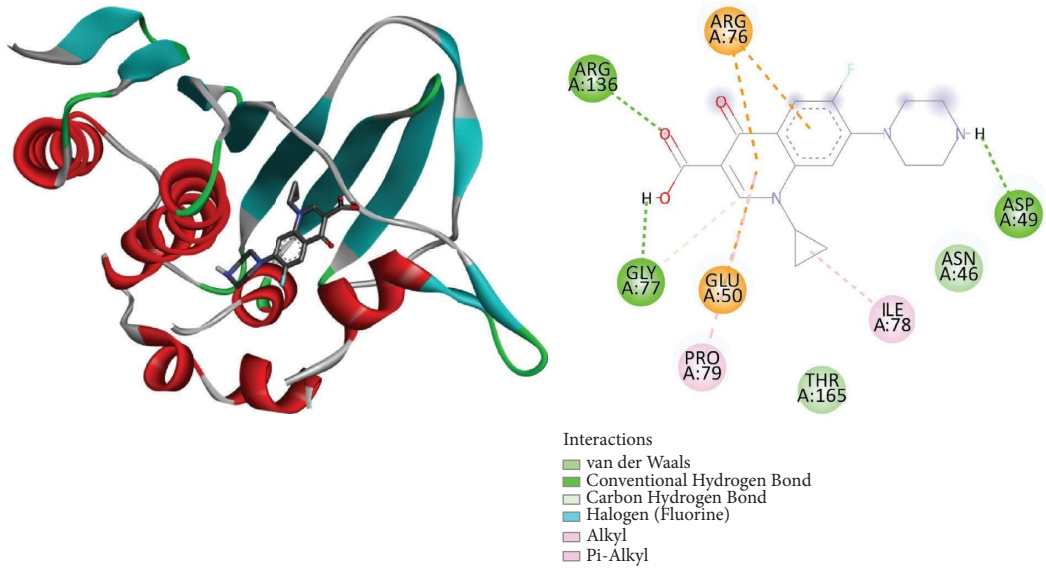

Figure 21: The binding interactions of ciprofloxacin against DNA gyrase of *E. coli* (PDB: 6F86).

Compound **1**–**3**, **4**–**7**, and **8** presented log S values of −4.47 to −4.84, −7.50 to −9.57, and 0.76, respectively. According to Sepay et al. [48], log *S* values between 0 and −2 indicate very good solubility, −2 to −4 indicate good solubility, −4 and −6 indicate moderate solubility, and less than −6 indicate low solubility. Considering this model, we can conclude that compounds **1**, **2**, and **3** are moderately water-soluble, and compound **8** is likely to be very good water-soluble and promising for oral administration. The total polar surface area (TPSA) influences the permeability and bioavailability of a molecule. All the TPSA values of compounds (17.07–138.07) are found to be less than the cut-off value (140 Å2), which indicates their excellent absorption in the intestine. Compounds **1**–**3** and **8** met all the requirements of the physicochemical and ADMET data.

The skin absorption of molecules is indicated by the skin permeability value (K_p) in cm/s. The more negative the value of log K_p, the less skin absorption [23]. The skin permeability, K_p, values of all isolated compounds (−1.97 to −9.37 cm/s) infer low skin permeability. In addition to that, absorption and distribution of drug molecules are measured by gastrointestinal (GI) and blood brain barrier (BBB) permeation. The Swiss ADME prediction parameters (Table 9) have shown that compounds **1**, **2**, and **3** have high gastrointestinal (GI) absorption, and none of the compounds have blood brain barrier (BBB) permeation except for compound **1**. Many different drugs' absorption, distribution, and clearance are affected by the P-GP. Therefore, permeability glycoprotein substrate identification is crucial for the identification and optimization of potential medicines. The findings demonstrate that all isolated compounds were not substrates of permeability glycoprotein (P-gp) except for compounds **1**, **3**, and **8**. When CYP enzymes are inhibited, inhibitory drug metabolism is compromised. Understanding the interaction of compounds with cytochromes P450 enzymes is crucial for the liver's drug metabolism. The prediction result exhibits that all the compounds are found to be noninhibitors for CYP2C19 and

Table 8: Drug-likeness predictions of compounds 1–**8**, computed by Swiss ADME.

Cds	MW	TPSA (Å2)	R.B	H.A	H.D	L.V	log P (o/w)	Log S (ESOL)
1	356.41	75.99	2	5	2	0	3.18	−4.56
2	358.43	79.15	2	5	3	0	3.07	−4.84
3	490.54	138.07	4	9	5	0	2.92	−4.47
4	424.70	17.07	0	1	0	1	4.55	−8.14
5	426.72	20.23	0	1	1	1	4.77	−8.34
6	442.72	40.46	1	2	2	1	4.45	−7.50
7	604.86	86.99	5	5	3	2	5.12	−9.57
8	194.18	99.38	2	6	4	0	1.25	0.76

MW: molecular weight, TPSA: topological polar surface area, R.B: number of rotatable bonds, H.A: number of hydrogen bond acceptors, H.D: number of hydrogen bond donors, L.V: number of Lipinski's rule of 5 violations, log P (o/w) (ilogP): lipophilicity.

Table 9: ADME predictions of compounds **1**–**8**, computed by Swiss ADME and PreADMET.

Cpds	LogKp (cm/s)	GIA	BBB	Inhibitor interaction (Swiss ADME/PreADMET)					
				1. P-gp substrate	CYP1A2	CYP2C19	CYP2C9	CYP2D6	CYP3A4
1	−5.88	High	Yes	Yes	Yes	No	No	Yes	No
2	−5.60	High	No	No	No	No	No	Yes	No
3	−7.49	High	No	Yes	No	No	No	No	No
4	−1.97	Low	No	No	No	No	No	No	No
5	−2.30	Low	No	No	No	No	No	No	No
6	−3.39	Low	No	No	No	No	No	No	No
7	−3.00	Low	No	No	No	No	No	No	Yes
8	−9.37	Low	No	Yes	No	No	No	No	No

GI: gastrointestinal, BBB: blood brain barrier, P-gp: P-glycoprotein, and CYP: cytochrome-P.

Table 10: Toxicity prediction of compounds, computed by ProTox-II and OSIRIS property explorer.

Cpds	LD_{50} (mg/kg)	Toxicity class	Organ toxicity					
			Hepatotoxicity	Carcinotoxicity	Immunotoxicity	Mutagenicity	Cytotoxicity	Irritant
1	777	4	Inactive	Inactive	Active	Active	Inactive	NO
2	777	4	Inactive	Inactive	Inactive	Active	Inactive	NO
3	1448	4	Inactive	Inactive	Active	Inactive	Inactive	NO
4	5000	5	Inactive	Inactive	Inactive	Inactive	Inactive	NO
5	7000	6	Inactive	Inactive	Active	Inactive	Inactive	NO
6	2830	5	Inactive	Inactive	Active	Inactive	Inactive	NO
7	9960	6	Inactive	Inactive	Active	Inactive	Inactive	NO
8	23000	6	Inactive	Inactive	Inactive	Inactive	Inactive	NO

CYP2C9. Compound **1** is a potential inhibitor for CYP1A2, and compounds 2–8 are noninhibitors. For CYP2D6, the compounds **3**–**8** are noninhibitors, and the other compounds **1**-**2** are potential inhibitors. For CYP3A4, compounds **1**–**6** and **8** are noninhibitors, and compound **7** is a potential inhibitor. According to ADME prediction parameters, compounds **3** and **8** met all the requirements for pharmacokinetic properties. The toxicity assessment was evaluated using the OSIRIS property explorer and ProTox-II online server to obtain the values of LD_{50} and molecular target toxicity probabilities (Table 10).

The result of the predictions represents the probability of each molecule to causing toxicity over specific targets. Acute toxicity prediction results such as LD_{50} values and toxicity class classification (1 (toxic) to 6 (nontoxic)) reveal that the isolated compounds **1**–**4** and **6** have shown toxicity class classification 4 and 5, respectively, indicating harmful if swallowed. The results found for the compounds **5** (LD_{50} = 7000 mg/kg), **7** (LD_{50} = 9960 mg/kg), and **8** (LD_{50} = 23000 mg/kg) indicate that the dose administered in this study would not be toxic. The toxicological prediction gives results for endpoints such as hepatotoxicity, carcinogenicity, mutagenicity, immunogenicity, and cytotoxicity. All compounds were predicted to be nonhepatotoxic, noncytotoxic, noncarcinotoxic, and nonirritant. Compounds **2**, **4**, and **8** were predicted to be nonimmunotoxic,

and compounds **3**–**8** were to be nonmutagenic. However, the compounds **1**, **3**, **5**, **6**, and **7** have shown immunotoxicity, and compounds **1** and **2** were found to have mutagenicity.

3.5. Chemotaxonomic Significance. Previous phytochemical studies revealed that species of the *Myrica* genus are rich in diarylheptanoids, dihydrochalcones, triterpenoids, and flavonoids [49]. In our present study, eight compounds, including three diarylheptanoids derivatives (**1**, **2**, **3**), pentacyclic triterpenoid derivatives (**4**, **5**, **6**, **7**), and one pyranoside derivative (**8**), were isolated from the stem bark of *M. salicifolia*. Compound **7** (3*β*-*O*-*trans*-caffeoylisomyricadiol) was identified for the first time, and this is the first report of compounds **4**–**7** from *M. salicifolia*. Furthermore, compound **8** is reported here in the *Myrica* genera. The diarylheptanoids and triterpenoids have been previously isolated from the *Myrica* genera, including myricanone (**1**) [50], myricanol (**2**) [50], and myricanol-11-*O*-*β*-D xylopyranoside (**3**) [51] from *M. rubra*, taraxerone (**4**), taraxerol (**5**), and myricadiol (**6**) from *M. cerifera* [52, 53]. Thus, compounds **4**–**8** from *M. salicifolia*, suggesting that their occurrence could be used to verify the chemotaxonomic relationship of *M. salicifolia* and other species of *Myrica*, might serve as valuable chemotaxonomic makers for the identification of *M. salicifolia*. Comprehensive phytochemical investigations involving an expanded series of compounds could help define the chemotaxonomic significance of species belonging to the genus *Myrica*.

4. Conclusions

In this study, a new compound, 3*β*-*O*-*trans*-caffeoylisomyricadiol (**7**), was isolated from the chloroform-methanol extract of *M. salicifolia* stem bark for the first time. According to the results of the antioxidant test, compounds **2**, **3**, and **7** demonstrated high antioxidant activities compared to the others. It is noteworthy that compounds **7** and **8** have not been reported from the *Myrica* genus and therefore suggest new findings on the chemotaxonomic information of the genus and additional constituents for the chemical diversity of *M. salicifolia*. The present study also demonstrated that compounds **3** and **7** from the stem bark of *M. salicifolia* possessed modest antibacterial activity against four strains, and compound **2** showed very strong antioxidant activity based on antioxidant activity parameters. Of all the compounds docked, compound **7** showed better binding affinity, with the active site of PqsA protein of *P. aeruginosa* and pyruvate kinase (PK) enzyme of *S. aureus*, with inhibition constant (K_i) 0.04 μM and 0.03 μM, respectively. In silico pharmacokinetics studies showed that the isolated compounds **1**–**3** and **8** satisfy Lipinski's rule of five with zero violations. As a result, we deduced that the current study would bring a new scientific report on the new isolated compound and other compounds.

Abbreviations

ADMET: Absorption, distribution, metabolism, excretion, and toxicity
ATCC: American type culture collection
CLSI: Clinical and Laboratory Standards Institute
DHB: 2,5-dihydroxybenzoic acid
1D-NMR: One-dimensional nuclear magnetic resonance spectroscopy
2D-NMR: Two-dimensional nuclear magnetic resonance spectroscopy
% [DPPH]: Percent of DPPH concentration; DPPH: 2, 2-diphenyl-1-picrylhydrazyl
ESI-MS: Electrospray ionization mass spectroscopy
HR-ESI-MS: High resolution electrospray ionization mass spectroscopy
IC50: Half maximal inhibitory concentration
TLC: Thin layer chromatography
TMS: Tetramethylsilane
UV-Vis: Ultraviolet-visible.

Data Availability

The datasets used and analyzed during the current study are available from the corresponding author on reasonable request.

Conflicts of Interest

The authors declare that they have no conflicts of interest.

Authors' Contributions

ADG performed lab work, data analysis, and writing of the draft manuscript and reviewing; KGB conducted NMR measurements, data analysis, and reviewing; TBD conducted docking studies, editing, and reviewing; JOO performed editing and reviewing; EEY and MAD conducted conceptualization and supervision and collected resources. All authors have read and approved the final manuscript.

Acknowledgments

The Departments of Chemistry of Addis Ababa University and the University of Botswana are greatly acknowledged for providing all the necessary research facilities and support. Abraham Dilnesa is grateful to the Ethiopian Forest Development Institute for sponsoring his study.

Supplementary Materials

Mass spectra, ^{1}H, ^{13}C and 2D NMR spectra of compounds **1**–**8** are available as supplementary materials. (*Supplementary Materials*)

References

[1] L. Mbuya, H. P. Msanga, C. K. Ruffo, A. Birnie, and B. O. Tengnas, *Useful Trees and Shrubs for Tanzania. Identification, Propagation and Management for Agricultural and Pastoral Communities*, Regional Soil Conservation Unit (RSCU)/Swedish International Development Authority (SIDA), Nairobi, Kenya, 1994.

[2] J. O. Kokwaro, *Medicinal Plants of East Africa*, University of Nairobi Press, Nairobi, Kenya, 3rd edition, 2009.

[3] B. G Meniso, A. D Boru, and N. B Ganjinaboyina, "Phytochemical investigation and evaluation of antimicrobial activities of stem bark of Morella salicifolia," *Bulletin of the Chemical Society of Ethiopia*, vol. 33, no. 2, pp. 293–306, 2019.

[4] Z. D. Kifle, G. M. Adinew, M. G. Mengistie et al., "Evaluation of antimalarial activity of methanolic root extract of Myrica salicifolia A rich (myricaceae) against Plasmodium berghei-infected mice," *Journal of evidence-based integrative medicine*, vol. 25, Article ID 2515690X2092053, 2020.

[5] C. Schlage, C. Mabula, R. L. A. Mahunnah, and M. Heinrich, "Medicinal plants of the Washambaa (Tanzania): documentation and ethnopharmacological evaluation," *Plant biology*, vol. 2, no. 1, pp. 83–92, 2000.

[6] I. Hedberg, O. Hedberg, P. J. Madat, K. E. Mshigeni, E. N. Mshiu, and G. Samuelsson, "Inventory of plants used in traditional medicine in Tanzania. II. Plants of the families dilleniaceae—opiliaceae," *Journal of Ethnopharmacology*, vol. 9, no. 1, pp. 105–127, 1983.

[7] M. Kamatenesi-Mugisha and H. Oryem-Origa, "Traditional herbal remedies used in the management of sexual impotence and erectile dysfunction in western Uganda," *African Health Sciences*, vol. 5, no. 1, pp. 40–49, 2005.

[8] A. Teklay, B. Abera, and M. Giday, "An ethnobotanical study of medicinal plants used in Kilte Awulaelo District, Tigray Region of Ethiopia," *Journal of Ethnobiology and Ethnomedicine*, vol. 9, no. 1, p. 65, 2013.

[9] A. I. Marealle, E. Innocent, K. Andrae-Marobela et al., "Safety evaluation and bioassay-guided isolation of antimycobacterial compounds from Morella salicifolia root ethanolic extract," *Journal of Ethnopharmacology*, vol. 296, Article ID 115501, 2022.

[10] P. G. Kirira, G. M. Rukunga, A. W. Wanyonyi et al., "Antiplasmodial activity and toxicity of extracts of plants used in traditional malaria therapy in Meru and Kilifi Districts of Kenya," *Journal of Ethnopharmacology*, vol. 106, no. 3, pp. 403–407, 2006.

[11] K. Njung'e, G. Muriuki, J. W. Mwangi, and K. A. M. Kuria, "Analgesic and antipyretic effects of Myrica salicifolia (Myricaceae)," *Phytotherapy Research*, vol. 16, no. S1, pp. 73-74, 2002.

[12] Y. K. Emiru, G. Periasamy, A. Karim, N. Ur Rehman, and M. N. Ansari, "Evaluation of in vitro α-amylase inhibitory activity and antidiabetic effect of Myrica salicifolia in streptozotocin-induced diabetic mice," *Pakistan Journal of Pharmaceutical Sciences*, vol. 33, no. 4, pp. 1917–1926, 2020.

[13] N. U. Rehman, M. N. Ansari, A. H. Palla et al., "Myrica salicifolia Hochst ex A. Rich. suppress acetic acid-induced ulcerative colitis in rats by reducing TNF-alpha and interleukin-6, oxidative stress parameters and improving mucosal protection," *Human and Experimental Toxicology*, vol. 41, Article ID 096032712211025, 2022.

[14] A. Geyid, D. A. Abebe, A. Debella et al., "Screening of some medicinal plants of Ethiopia for their anti-microbial properties and chemical profiles," *Journal of Ethnopharmacology*, vol. 97, no. 3, pp. 421–427, 2005.

[15] E. Makule, T. Schmidt, J. Heilmann, and B. Kraus, "Diarylheptanoid glycosides of Morella salicifolia bark," *Molecules*, vol. 22, no. 12, p. 2266, 2017.

[16] D. K. Isika, F. N. Özkömeç, M. Çeşme, and O. A. Sadik, "Synthesis, biological and computational studies of flavonoid acetamide derivatives," *Royal Society of Chemistry Advances*, vol. 12, no. 16, pp. 10037–10050, 2022.

[17] AAT Bioquest, "IC50 Calculator," 2023, https://www.aatbio.com/tools/ic50-calculator.

[18] P. Wayne, "National committee for clinical laboratory standards," *Performance Standards For Antimicrobial Disc Susceptibility Testing*, vol. 12, pp. 1–53, 2002.

[19] K. Ohemeng, C. F. Schwender, K. P. Fu, and J. F. Barrett, "DNA gyrase inhibitory and antibacterial activity of some flavones (1)," *Bioorganic and Medicinal Chemistry Letters*, vol. 3, no. 2, pp. 225–230, 1993.

[20] E. N. Okolo, D. I. Ugwu, B. E. Ezema et al., "New chalcone derivatives as potential antimicrobial and antioxidant agent," *Scientific Reports*, vol. 11, no. 1, Article ID 21781, 2021.

[21] K. Konaté, J. F. Mavoungou, A. N. Lepengué et al., "Antibacterial activity against β- lactamase producing methicillin and ampicillin-resistants *Staphylococcus aureus*: fractional inhibitory concentration index (FICI) determination," *Annals of Clinical Microbiology and Antimicrobials*, vol. 11, p. 18, 2012.

[22] G. M. Morris, R. Huey, W. Lindstrom et al., "AutoDock4 and AutoDockTools4: automated docking with selective receptor flexibility," *Journal of Computational Chemistry*, vol. 30, no. 16, pp. 2785–2791, 2009.

[23] A. Daina, O. Michielin, and V. Zoete, "SwissADME: a free web tool to evaluate pharmacokinetics, drug-likeness and medicinal chemistry friendliness of small molecules," *Scientific Reports*, vol. 7, no. 1, Article ID 42717, 2017.

[24] M. N. Drwal, P. Banerjee, M. Dunkel, M. R. Wettig, and R. Preissner, "ProTox: a web server for the in silico prediction of rodent oral toxicity," *Nucleic Acids Research*, vol. 42, no. W1, pp. W53–W58, 2014.

[25] B. S. Joshi, S. W. Pelletier, M. G. Newton, D. Lee, G. B. McGaughey, and M. S. Puar, "Extensive 1D, 2D NMR spectra of some [7.0]Metacyclophanes and X-ray analysis of (±)-Myricanol," *Journal of Natural Products*, vol. 59, no. 8, pp. 759–764, 1996.

[26] M. Tene, H. K. Wabo, P. Kamnaing et al., "Diarylheptanoids from Myrica arborea," *Phytochemistry*, vol. 54, no. 8, pp. 975–978, 2000.

[27] N. Trimedona, H. Nurdin, D. Darwis, and M. Efdi, "Isolation of triterpenoid from stem bark of Pometia pinnata, Forst & Forst," *Journal of Chemical and Pharmaceutical Research*, vol. 7, pp. 225–227, 2015.

[28] M. E. Abouelela, M. A. Orabi, R. A. Abdelhamid, M. S. Abdelkader, and F. M. Darwish, "Chemical and cytotoxic investigation of non-polar extract from Ceiba pentandra (L.) Gaertn.: a study supported by computer based screening," *Journal of Applied Pharmaceutical Science*, vol. 8, no. 7, pp. 57–064, 2018.

[29] I. Merfort, J. Buddrus, M. A. M. Nawwar, and J. Lambert, "A triterpene from the bark of Tamarix aphylla," *Phytochemistry*, vol. 31, no. 11, pp. 4031-4032, 1992.

[30] T. E. Walker, R. E. London, T. W. Whaley, R. Barker, and N. A. Matwiyoff, "Carbon-13 nuclear magnetic resonance spectroscopy of [1-13C] enriched monosaccharides. Signal assignments and orientational dependence of geminal and vicinal carbon-carbon and carbon-hydrogen spin-spin coupling constants," *Journal of the American Chemical Society*, vol. 98, no. 19, pp. 5807–5813, 1976.

[31] M. U. Roslund, P. Tähtinen, M. Niemitz, and R. Sjöholm, "Complete assignments of the 1H and 13C chemical shifts and JH, H coupling constants in NMR spectra of D-glucopyranose and all D-glucopyranosyl-D-glucopyranosides," *Carbohydrate Research*, vol. 343, no. 1, pp. 101–112, 2008.

[32] P. Charisiadis, V. Kontogianni, C. Tsiafoulis, A. Tzakos, M. Siskos, and I. P. Gerothanassis, "1H-NMR as a structural and analytical tool of intra- and intermolecular hydrogen bonds of phenol-containing natural products and model compounds," *Molecules*, vol. 19, no. 9, pp. 13643–13682, 2014.

[33] S. De Marino, M. Iorizzi, F. Zollo et al., "Isolation, structure elucidation, and biological activity of the steroid oligoglycosides and polyhydroxysteroids from the Antarctic starfish Acodontaster conspicuus," *Journal of Natural Products*, vol. 60, no. 10, pp. 959–966, 1997.

[34] E. N. Drake and C. E. Brown, "Application of nmr to biochemical kinetics. A laboratory experiment in physical biochemistry," *Journal of Chemical Education*, vol. 54, no. 2, p. 124, 1977.

[35] R. S. Orfali, S. S. Ebada, A. M. El-Shafae et al., "3-O-trans-caffeoylisomyricadiol: a new triterpenoid from Tamarix nilotica growing in Saudi Arabia," *Zeitschrift für Naturforschung C*, vol. 64, no. 9–10, pp. 637–643, 2009.

[36] Y. Jin, Y. Xu, Z. Huang, Z. Zhou, and X. Wei, "Metabolite pattern in root nodules of the actinorhizal plant *Casuarina equisetifolia*," *Phytochemistry*, vol. 186, Article ID 112724, 2021.

[37] S. Laphookhieo, C. Karalai, C. Ponglimanont, and K. Chantrapromma, "Pentacyclic triterpenoid esters from the fruits of Bruguiera c ylindrica," *Journal of Natural Products*, vol. 67, no. 5, pp. 886–888, 2004.

[38] R. Reviana, A. N. Usman, I. Raya et al., "Analysis of antioxidant activity on cocktail honey products as female preconception supplements," *Gaceta Sanitaria*, vol. 35, no. Suppl 2, pp. S202–S205, 2021.

[39] J. C. R. Vellosa, L. O. Regasini, N. M. Khalil et al., "Antioxidant and cytotoxic studies for kaempferol, quercetin and isoquercitrin," *Eclética Química*, vol. 36, no. 2, pp. 07–20, 2011.

[40] D. Rusmana, R. Wahyudianingsih, M. Elisabeth, B. Balqis, M. Maesaroh, and W. Widowati, "Antioxidant activity of Phyllanthus niruri extract, rutin and quercetin," *The Indonesian Biomedical Journal*, vol. 9, no. 2, p. 84, 2017.

[41] T. Damena, M. B. Alem, D. Zeleke, T. Desalegn, R. Eswaramoorthy, and T. B. Demissie, "Novel zinc(II) and copper(II) complexes of 2-((2-hydroxyethyl)amino)quinoline-3-carbaldehyde for antibacterial and antioxidant activities: a combined experimental, DFT, and docking studies," *American Chemical Society Omega*, vol. 7, no. 30, pp. 26336–26352, 2022.

[42] S. Inouye, T. Takizawa, and H. Yamaguchi, "Antibacterial activity of essential oils and their major constituents against respiratory tract pathogens by gaseous contact," *Journal of Antimicrobial Chemotherapy*, vol. 47, no. 5, pp. 565–573, 2001.

[43] M. Miklasińska-Majdanik, M. Kępa, R. D. Wojtyczka, D. Idzik, and T. J. Wąsik, "Phenolic compounds diminish antibiotic resistance of *Staphylococcus aureus* clinical strains," *International Journal of Environmental Research and Public Health*, vol. 15, no. 10, p. 2321, 2018.

[44] T. Gonfa, A. Temesgen, O. Erba, E. T. Mengesha, and M. Sivasubramanian, "Phytochemicals analysis, in vitro antibacterial activities of extracts, and molecular docking studies of the isolated compounds from Melhania zavattarii Cufod leaves," *Journal of Tropical Medicine*, vol. 2023, Article ID 8820543, 12 pages, 2023.

[45] B. Mekonnen Sanka, D. Mamo Tadesse, E. Teju Bedada, E. T. Mengesha, and N. Babu G, "Design, synthesis, biological screening and molecular docking studies of novel multifunctional 1,4-di (aryl/heteroaryl) substituted piperazine derivatives as potential antitubercular and antimicrobial agents," *Bioorganic Chemistry*, vol. 119, Article ID 105568, 2022.

[46] C. A. Lipinski, F. Lombardo, B. W. Dominy, and P. J. Feeney, "Experimental and computational approaches to estimate solubility and permeability in drug discovery and development settings," *Advanced Drug Delivery Reviews*, vol. 64, pp. 4–17, 2012.

[47] A. Ah and A. Yi, "In silico pharmacokinetics and molecular docking studies of lead compounds derived from Diospyros mespiliformis," *Pharma*, vol. 7, no. 3, p. 31, 2019.

[48] N. Sepay, N. Sepay, A. Al Hoque, R. Mondal, U. C. Halder, and M. Muddassir, "In silico fight against novel coronavirus by finding chromone derivatives as inhibitor of coronavirus main proteases enzyme," *Structural Chemistry*, vol. 31, no. 5, pp. 1831–1840, 2020.

[49] G. P. Rosa, B. J. C. Silva, A. M. L. Seca, L. M. Moujir, and M. C. Barreto, "Phytochemicals with added value from Morella and Myrica species," *Molecules*, vol. 25, no. 24, p. 6052, 2020.

[50] S. Shen, M. Zhao, C. Li et al., "Study on the material basis of neuroprotection of Myrica rubra bark," *Molecules*, vol. 24, no. 16, p. 2993, 2019.

[51] J. Tao, T. Morikawa, I. Toguchida, S. Ando, H. Matsuda, and M. Yoshikawa, "Inhibitors of nitric oxide production from the bark of Myrica rubra: structures of new biphenyl type diarylheptanoid glycosides and taraxerane type triterpene," *Bioorganic and Medicinal Chemistry*, vol. 10, no. 12, pp. 4005–4012, 2002.

[52] B. D. Paul, G. Subba Rao, and G. J. Kapadia, "Isolation of myricadiol, myricitrin, taraxerol, and taraxerone from Myrica cerifera L. root bark," *Journal of Pharmaceutical Sciences*, vol. 63, no. 6, pp. 958-959, 1974.

[53] N. Sakurai, Y. Hosono, M. Morihara et al., "A new triterpenoid myricalactone and others from Myrica gale var. tomentosa," *Journal of the Pharmaceutical Society of Japan*, vol. 117, no. 4, pp. 211–219, 1997.